Redox Biology 63 (2023) 102711

Contents lists available at ScienceDirect

Redox Biology

journal homepage: www.elsevier.com/locate/redox

NFATc1-mediated expression of SLC7A11 drives sensitivity to TXNRD1 inhibitors in osteoclast precursors

Zeyuan Zhong [a,b,1], Chongjing Zhang [a,b,1], Shuo Ni [c,1], Miao Ma [d], Xiaomeng Zhang [e], Weicong Sang [b], Tao Lv [a], Zhi Qian [f,***], Chengqing Yi [a,**], Baoqing Yu [g,*]

[a] Department of Orthopedics, Shanghai Pudong Hospital, Fudan University Pudong Medical Center, Shanghai, China
[b] Shanghai Medical College, Fudan University, Shanghai, China
[c] Department of Orthopedic Surgery and Shanghai Institute of Microsurgery on Extremities, Shanghai Jiaotong University Affiliated Sixth People's Hospital, Shanghai, China
[d] The Second Clinical Medical College, Lanzhou University, Lanzhou, China
[e] Renal Medicine and Baxter Novum, CLINTEC, Karolinska Institutet, Stockholm, Sweden
[f] Institution of Orthopaedic Diseases, Zhangye People's Hospital Affiliated to Hexi University, Zhangye, China
[g] Department of Orthopedics, Shanghai Pudong New Area People's Hospital, Shanghai, China

ARTICLE INFO

Keywords:
Metabolic reprogramming
Osteoclast
NFATc1
TXNRD1
SLC7A11
Disulfidptosis

ABSTRACT

Excess osteoclast activity is found in many bone metabolic diseases, and inhibiting osteoclast differentiation has proven to be an effective strategy. Here, we revealed that osteoclast precursors (pre-OCs) were more susceptible to thioredoxin reductase 1 (TXNRD1) inhibitors than bone marrow-derived monocytes (BMDMs) during receptor activator of nuclear factor kappa B ligand (RANKL)-mediated osteoclastogenesis. Mechanistically, we found that nuclear factor of activated T-cells 1 (NFATc1) upregulated solute carrier family 7 member 11 (SLC7A11) expression through transcriptional regulation during RANKL-induced osteoclastogenesis. During TXNRD1 inhibition, the rate of intracellular disulfide reduction is significantly reduced. Increased cystine transport leads to increased cystine accumulation, which leads to increased cellular disulfide stress and disulfidptosis. We further demonstrated that SLC7A11 inhibitors and treatments that prevent disulphide accumulation could rescue this type of cell death, but not the ferroptosis inhibitors (DFO, Ferro-1), the ROS scavengers (Trolox, Tempol), the apoptosis inhibitor (Z-VAD), the necroptosis inhibitor (Nec-1), or the autophagy inhibitor (CQ). An *in vivo* study indicated that TXNRD1 inhibitors increased bone cystine content, reduced the number of osteoclasts, and alleviated bone loss in an ovariectomized (OVX) mouse model. Together, our findings demonstrate that NFATc1-mediated upregulation of SLC7A11 induces targetable metabolic sensitivity to TXNRD1 inhibitors during osteoclast differentiation. Moreover, we innovatively suggest that TXNRD1 inhibitors, a classic drug for osteoclast-related diseases, selectively kill pre-OCs by inducing intracellular cystine accumulation and subsequent disulfidptosis.

1. Introduction

Osteoclast overactivity is a feature of many diseases, such as rheumatoid arthritis, osteoporosis, and bone metastasis. In these diseases, mature osteoclasts (ma-OCs) exert bone-destructive effects through bone resorption [1–6]. Inhibiting osteoclast differentiation has proven to be an effective therapeutic strategy in basic research and clinical treatment [1,7–10]. During osteoclast differentiation, bone marrow-derived monocytes (BMDMs) undergo metabolic reprogramming in response to the stimulation of receptor activator of nuclear factor kappa B ligand (RANKL) and other cytokines. This process renders osteoclast precursors (pre-OCs) highly dependent on specific nutrients for survival and differentiation, compared to BMDMs [11–13]. Limiting these nutrients uptake or dampening their metabolic processes may inhibit the osteoclastogenesis or selectively kill pre-OCs. However, while

* Corresponding author.
** Corresponding author.
*** Corresponding author.
E-mail addresses: zqian16@fudan.edu.cn (Z. Qian), ycq3000@126.com (C. Yi), doctorybq@163.com (B. Yu).
[1] These authors contributed equally to this article.

https://doi.org/10.1016/j.redox.2023.102711
Received 5 April 2023; Accepted 21 April 2023
Available online 29 April 2023

Abbreviations:

2 ME	2-mercaptoethanol
Acp5	Acid Phosphatase 5
AF	Auranofin
BMD	bone mineral density
BMDMs	bone marrow-derived monocytes
BMSCs	bone marrow stromal cells
BV/TV	bone volume per tissue volume
CQ	Chloroquine
Cs. Th	cortical thickness
CTL	control
CTX-1	C-terminal telopeptide of type I collagen
CUT & Tag	Cleavage under targets and tagmentation
DFO	Deferoxamine
EV	Empty vector
F-actin	actin filaments
Ferro-1	ferrostatin-1
GO	Gene Ontology
GSH	glutathione
H&E	hematoxylin-eosin staining
HPLC−MS/MS	High-performance liquid chromatography-tandem mass spectrometry
KEAP1	kelch like ECH associated protein 1
KO	knockout
LC-MS	Liquid Chromatographic Mass Spectrometer
L-Pen	L-Penicillamine
ma-OCs	mature osteoclast
MAR	mineral apposition rate
M-CSF	macrophage colony-stimulating factor
MFI	mean fluorescence intensity
NAC	N-acetylcysteine
Nec-1	Necrostatin-1
NFATc1	nuclear factor of activated T-cells 1
NMR	Nuclear Magnetic Resonance
NRF2	NF-E2-related factor 2
ROS	reactive oxygen species
RANKL	receptor activator of nuclear factor kappa B ligand
OVX	ovariectomized
PB	periosteal bone
PCA	Principal component analysis
PDGF-BB	platelet-derived growth factor beta polypeptide b
PI	propidium iodide
pre-OCs	osteoclast precursors
ROS	reactive oxygen species
RSL3	(1S,3R)-RSL3
SLC7A11	solute carrier family 7 member 11
SSZ	sulfasalazine
TB	trabecular bone
Tb·N	number of trabeculae
Tb. Sp	trabecular separation
TRAP	tartrate resistance acid phosphatase
TRi-1	TXNRD1 inhibitor 1
Trx	thioredoxin
TSSs	transcription start sites
TXNRD1	thioredoxin reductase 1
TXNRD2	thioredoxin reductase 2
TXNRDs	thioredoxin reductases
WT	Wild type
Z-VAD	Z-VAD-FMK

therapies targeting metabolic vulnerabilities have been widely used in cancer treatment [14–16], selective killing of pre-OCs has rarely been investigated as a potential treatment for osteoclast-related diseases.

Cysteine is a nonessential amino acid and is indispensable for multiple biological processes [17]. Cysteine is the rate-limiting precursor for synthesizing glutathione (GSH), one of the most crucial cellular antioxidants. Under physiological conditions, cysteine can be synthesized via the transsulfuration pathway or proteolysis. However, cells with high cysteine demand or lacking the transsulfuration pathway obtain cysteine mainly from the extracellular environment via amino acid transporters. Since cysteine has a reduced thiol group, it will be oxidized to cystine (cysteine in dimeric form with a disulphide bond) in the oxidizing extracellular environment within 30 min [18]. Under this condition, the cells import cystine via solute carrier family 7 member 11 (SLC7A11) [19] and then reduce the oxidizing cystine to cysteine by the thioredoxin system [20,21]. The thioredoxin system and glutathione systems contribute to antioxidant defence systems in mammals. The thioredoxin system exerts antioxidative properties by reducing disulphide to dithiol [22–24]. Without TXNRD1, intracellular cystine with a disulphide bond cannot be reduced to cysteine with a thiol group [21,22]. Due to the extremely low solubility of cystine (less than 1/2000 of cysteine), imported cystine tends to accumulate in cells, increasing cellular disulfide stress [18]. Under high disulphide metabolic stress, aberrant disulphide bonds are formed in actin cytoskeletal proteins, leading to cell death [25]. Selenoprotein thioredoxin reductase 1 (TXNRD1) is the most common target for inhibiting the thioredoxin system at present [21,26,27]. Auranofin (AF, also called Ridaura®), a drug approved by the FDA in 1985 for the treatment of rheumatoid arthritis [28], has been investigated due to its antitumor activity mediated by targeting TXNRD1 [29–31]. Nevertheless, a number of previous studies have focused on the anti-inflammatory role of AF in osteoclast-related diseases [32–35], while its inhibition of TXNRD1 in this field has not been reported. As a canonical inhibitor of TXNRDs, AF not only binds TXNRD1 but also inhibits the mitochondrial enzyme TXNRD2, glutathione S-transferase, and several phosphatases [35–37]. Recently, more specific targeting drugs have been developed to validate TXNRD1 as a therapeutic target. Among these, TXNRD1 inhibitor 1 (TRi-1) is notable for its specific binding ability to TXNRD1 and has been utilized in some basic studies [27,38].

We reveal that nuclear factor of activated T-cells 1 (NFATc1) regulates SLC7A11 expression via transcription during RANKL-mediated osteoclast differentiation. Metabolic reprogramming of cystine uptake renders pre-OCs more vulnerable to TXNRD1 inhibitor-induced cell death than BMDMs. We further demonstrate that increased cystine uptake leads to F-actin contraction, which mediates disulfidptosis in pre-OCs under TXNRD1 inhibition. Our study elucidates the underlying mechanisms of TXNRD1 inhibitors for the treatment of osteoclast-related diseases and proposes selective killing of pre-OCs as a feasible therapeutic strategy for diseases with osteoclast overactivity.

2. Materials and methods

2.1. Isolation and culture of BMDMs

BMDMs were isolated from wild-type or SLC7A11$^{-/-}$ mice as previously described [39]. Briefly, 4-week-old C57BL/6J mice were dissected under Zoletil 50 (50 mg/kg) anaesthesia, and the tibiae and femora were collected. The bones were flushed using a syringe filled with α–minimum essential medium containing 10% fetal bovine serum (VWR, Australia) and 40 ng/mL murine macrophage colony-stimulating factor (M-CSF) (R&D, USA) to obtain bone marrow cells. The suspended cells were collected in 10 cm dishes, and the medium was replaced every 48 h. After 96 h, the adherent cells were washed three times with PBS and identified by flow cytometry using FITC-F4/80 (BioLegend, USA)

and APC-CD11b (BioLegend, USA) antibodies.

2.2. Preparation of pre-OCs and ma-OCs

Harvested BMDMs were cultured at a density of 8×10^3/well (96-well plates) or 4×10^5/well (6-well plates) in a medium containing 20 ng/mL M-CSF (R&D, USA) and 50 ng/mL RANKL (R&D, USA).The medium was replaced every 48 h. After 72 h, pre-OCs were identified using a TRAP staining kit (Sigma-Aldrich, USA). The pre-OCs were further induced with a medium containing 20 ng/mL M-CSF and 50 ng/mL RANKL for two days. TRAP staining (Sigma−Aldrich, USA) and F-actin formation assays (Yeasen, China) were performed to assess osteoclast differentiation and fusion.

2.3. Mice and experimental surgery

C57BL/6 wild-type mice were provided by Suzhou Syagen Laboratory Animal Co., Ltd. SLC7A11 knockout mice were generated using the CRISPR/Cas9 system in the C57BL/6J mouse strain, and SLC7A11$^{-/-}$ generation was performed by the Suzhou Syagen Laboratory Animal Co., Ltd (Fig. S2a). The exon 3 of the *Slc7a11* gene (NCBI Reference Sequence: NM_011990.2; Ensembl: ENSMUSG000-00027737) was the target of guide RNAs (gRNAs). Then, the mouse zygotes were microinjected with Cas9 mRNA and gRNAs. The following primers were used to detect the F0 generation pups by PCR: Primers 1, F1, 5′-TACTGTGATAAGCAGTGTAGAGGG-3′, R1, 5′-GTTATAGGAAATGGCCGTCAGATG-3’; Primers 2, F1, 5′-TACTGTGATAAGCAGTGTAGAGGG-3′, R2, 5′-AGAGACCAACCCATATT-ACCTGAC-3’ (Fig. S2b). The Animal Ethics Committee of Fudan University Pudong Medical Center approved this study (No. 20220725-1), and all animal experiments were conducted in accordance with the National Institutes of Health (NIH, USA) Guide for the Care and Use of Laboratory. All female mice at 8 weeks old were randomly divided into a sham group, an ovariectomized (OVX) group, an AF group, and a TRi-1 group (n = 6). In the OVX, AF, and TRi-1 groups, bilateral OVX was performed through a dorsal approach under the anaesthesia of 50 mg/kg Zoletil 50. For the sham group, paraovarian adipose tissues were removed via the same approach. After three days, in the sham and OVX groups, PBS containing 2% DMSO was administered intraperitoneally. The AF group received AF (10 mg/kg) dissolved in PBS containing 2% DMSO. The TRi-1 group received TRi-1 (5 mg/kg) dissolved in PBS containing 2% DMSO every two days for eight weeks. Mice were injected with calcein (10 mg/kg) ten days and three days before sacrifice. Body weights were recorded weekly. After eight weeks, the bilateral tibiae, bilateral femora, and sera of the mice were collected for the subsequent experiments. The uteruses of the mice were measured. Hematoxylin-eosin (H&E) staining of mice viscera was used to assess the drug toxicity in this study.

2.4. Bone resorption assay in vitro

Bone resorption activity was assessed as described previously [39]. Briefly, BMDMs were seeded onto bone slices in 96-well plates at a density of 8000 cells/well, then cultured for seven days with a medium containing 20 ng/mL M-CSF and 50 ng/mL RANKL. The bone slices were removed and ultrasonicated to remove adherent cells, and the surfaces were scanned with an electron microscope (GeminiSEM 500, Germany). Quantification was achieved by measuring the percentage of the areas resorbed in three random views using ImageJ software (NIH, USA).

2.5. Flow cytometry

Bone marrow cells were collected in 10 cm dishes and cultured with M-CSF for 96 h. We washed adherent cells three times with PBS and incubated them with FITC-F4/80 (BioLegend, USA) and APC-CD11b (BioLegend, USA) antibodies. A fluorescence-activated cell sorter (FACSCanto II, BD) was used for analyses, and CD11b$^+$F4/80$^+$ cells were considered BMDMs.

To measure cystine uptake of BMDMs, pre-OCs, and ma-OCs, cells were cultured with cystine-free medium for 1 h. After cystine starvation, the cells were incubated with 5 μM cystine-FITC probes (Sigma-Aldrich, USA) for 1 h, and the flow cytometry was used to analyse the fluorescence intensity. For fluorescent photos, the cells were incubated with 150 μM cystine-FITC probes for 4 h.

To measure cell death, 4×10^5 cells/well were seeded in 6-well plates one day before treatment. Cells were harvested 24 h after different treatments and incubated with 10 μL/mL propidium iodide (PI) solution (BioLegend, USA) at 4 °C for 15 min and measured by flow cytometry.

Cellular lipid peroxidation was assessed using Liperfluo (Dojindo, Japan). One day before treatment, 4×10^5 cells/well were seeded in 6-well plates. Cells were harvested 24 h after different treatments. After incubation with 1 μM Liperfluo for 30 min, the cells were measured by flow cytometry.

ROS Brite 570 (AAT Bioquest, USA) staining was used to detect cellular ROS. One day before treatment, 4×10^5 cells/well were seeded in 6-well plates. Cells were harvested 5 h after different treatments. After incubation with 5 μL/mL100 × ROS Brite 570 stock solution for 30 min, the cells were measured by flow cytometry.

2.6. Detection of TXNRDs reduction ability

Reduction of TRFS-Green (MedChemExpress, USA) by the combination of various Trx system components was performed after the cells were pretreated with or without TXNRDs inhibitors [40]. In brief, first, BMDMs and pre-OCs were pretreated with a medium containing no drug, AF (0.5 μM, 1.0 μM) or TRI-1 (1.0 μM, 2.0 μM) for 3 h. Then, the pretreated cells were incubated with TRFS (10 μM) for 2 h. The fluorescence of the cells was detected with a fluorescence microscope (Nikon, Japan).

2.7. Liquid chromatographic mass spectrometer (LC-MS) analysis

The identified BMDMs and pre-OCs (1×10^7 cells per sample) were washed with PBS. A 1:1 mixture of methanol and acetonitrile (1:1, v/v) was used to remove the protein and extract the metabolites. The mixture was centrifuged to collect the supernatant. After vacuum centrifugation, the supernatant was dried, then redissolved in acetonitrile: water (1:1, v/v) solvent for LC-MS analysis. For untargeted metabolomics of polar metabolites, extracts were analysed using a quadrupole time-of-flight mass spectrometer (Sciex TripleTOF 6600) coupled to hydrophilic interaction chromatography via electrospray ionization in Shanghai Applied Protein Technology Co., Ltd. LC separation was performed on an ACQUIY UPLC BEH Amide column with a gradient of solvent A (25 mM ammonium acetate and 25 mM ammonium hydroxide in water) and solvent B (acetonitrile). The gradient was 85% B for 1 min and was linearly reduced to 65% in 11 min, then reduced to 40% in 0.1 min and kept for 4 min, and then increased to 85% in 0.1 min, with a 5 min re-equilibration period employed. The mass spectrometer was operated in both negative ion and positive ionization modes. In MS acquisition, the instrument was set to acquire over the *m/z* range of 60–1000 Da, and the accumulation time for the TOF MS scan was set at 0.20 s/spectra. The product ion scan is acquired using information-dependent acquisition (IDA) with high sensitivity mode selected.

2.8. High-performance liquid chromatography-tandem mass spectrometry (HPLC−MS/MS)

The intracellular cystine levels were detected by HPLC-MS/MS as described previously with modification [18,41]. Briefly, to ensure that the cell amounts were consistent among groups, the treated cells were digested by trypsin and counted by a cell counter (Beckman, USA). Then, the cells were centrifuged, resuspended with pre-cooled PBS,

centrifuged again, and the supernatant was removed. Resuspend the cells with pre-cooled extraction buffer consisting of 40% methanol, 40% acetonitrile, and 20% water containing 100 mM formic acid and 1 mM EDTA and detect the cystine level by HPLC-MS/MS. For bone samples, the same protocol was followed as for cell samples after weighing and grinding. The same method was used to detect intracellular GSH and GSSG levels.

2.9. Cleavage under targets and tagmentation (CUT & Tag)

The CUT&Tag assay was performed as described previously with modifications [42]. Briefly, 5×10^5 pre-OCs were washed twice gently with wash buffer. Each sample was incubated with 10 μL of concanavalin A-coated magnetic beads (Bangs Laboratories) at RT for 10 min. The unbound supernatant was removed, and bead-bound cells were resuspended with dig wash buffer (20 mM HEPES pH 7.5; 150 mM NaCl; 0.5 mM spermidine; 1 × protease inhibitor cocktail; 0.05% digitonin; 2 mM EDTA) and a 1:50 dilution of primary antibody or normal mouse IgG (1:100, 12–371, Millipore) incubated on a rotating platform overnight at 4 °C. The primary antibody was removed using a magnet stand. The cells were incubated with rabbit anti-mouse IgG H&L (1:100, ab611709, Abcam) at RT for 60 min and washed with wash buffer on a magnet stand for 2–3 times. The pA-Tn5 adapter complex (1:100) was prepared in dig-med buffer (0.01% digitonin; 20 mM HEPES pH 7.5; 300 mM NaCl; 0.5 mM spermidine; 1 × protease inhibitor cocktail) and incubated with cells at RT for 1 h. Cells were washed with Dig-Med buffer 2–3 times. Then, we resuspended the cells in tagmentation buffer (10 mM $MgCl_2$ in Dig-Med Buffer) and incubated them for 1 h at 37 °C. Phenol−chloroform-isoamyl alcohol extraction and ethanol precipitation were used for DNA purification. For the amplification of libraries, we mixed 21 μL of DNA, 2 μL of a universal i5, and a uniquely barcoded i7 primer. A volume of 25 μL of NEBNext HiFi 2 × PCR Master mix was added and mixed. The sample was placed in a Thermocycler with a heated lid using the following cycling conditions: 72 °C for 5 min (gap filling); 98 °C for 30 s; 14 cycles of 98 °C for 10 s and 63 °C for 30 s; final extension at 72 °C for 1 min and hold at 8 °C. Library clean-up was performed with XP beads (Beckman, Germany).

2.10. Luciferase assay

A SLC7A11 promoter fragment (202 base pairs, spanning from 50443437 to 50443638, chr3, GRCm38) was amplified by PCR and cloned into the KpnI and XhoI sites of pGL3-Basic to construct the reporter vectors. We confirmed the nucleotide sequences of the DNA fragments cloned into the reporter vectors by Sanger sequencing. The obtained vectors, together with the NFATc1 overexpression vector, were co-transfected into MC3T3-E1 cells using Lipo3000 (Invitrogen, Canada). In the mutant group, we constructed the reporter vector by mutating the predicted binding sequence 5′-TTTC-3′to 5′-CCCT-3′ to Forty-eight hours after transfection, a dual luciferase reporter system (Vazyme, China) was used to measure the luciferase activity in the cell extracts according to the manufacturer's instructions.

2.11. ELISA

Blood was collected from mice and clotted overnight at 4 °C before centrifuging for 20 min at 3000 rpm, and sera were subpackaged and stored at −80 °C for subsequent assays. The concentrations of the C-terminal peptide of type I collagen (CTX-1) in mouse sera were examined with a mouse ELISA kit (MULTISCIENCES, China).

2.12. Cell viability assay

Cell viability was measured using a commercially available CCK-8 kit (Dojindo, Japan) according to the manufacturer's instructions. Briefly, 2×10^4 cells/well were seeded into 96-well plates one day before treatment. The medium was replaced with 100 μL CCK-8 working solution (10 μL CCK-8 solution, 90 μL α-MEM) after different treatments. After incubation in a cell incubator for 1 h, the absorbance (450 nm) of each well was detected using a microplate reader (Infinite 200 pro, Tecan, Switzerland).

2.13. Antibodies, primers, and reagents

The primary antibodies for Western blot analyses were mouse anti-NFATc1 (1: 100, sc-7294, Santa Cruz), rabbit anti-SLC7A11 (1: 1000, A2413, ABclonal), rabbit anti-NRF2 (1:10000, 16396-1-AP, Proteintech), rabbit anti-KEAP1 (1:5000, 10503-2-AP, Proteintech), rabbit anti–HO–1 (1: 5000, A19062, ABclonal),rabbit anti-TXNRD1 (1:1000, A4725, ABclonal), rabbit anti-Vinculin (1: 1000, A2752, ABclonal), rabbit anti-β-Actin (1: 1000, AC006, ABclonal). The secondary antibodies were horseradish peroxidase-conjugated goat anti-rabbit (1:3000; 7074, Cell Signaling) and horseradish peroxidase-conjugated goat anti-mouse (1:3000; 7076, Cell Signaling). The primers used for PCR were as follows: *Slc7a11*, Primers 1, 5′-GGTGGAACTGCTCGTAAT-3' (forward) and 5′-GCTGACACTCGTGCTATT-3' (reverse); *Slc7a11*, Primers 2, 5′-ATCTCCCCCAAGGGCATACT-3' (forward) and 5′-GCATAGGACAGGGCT-CCAAA-3' (reverse); *Nfatc1*, 5′-CTGGTCTTCCGAGTTCAC-3' (forward) and 5′-GTCTGTGCTCTGCTTCTC-3' (reverse); *Txnrd1*, 5′-CGAGAACTATTGGCTTAGAGA-3' (forward) and 5′-ACCGATGGCGTAGATGTA-3' (reverse); *Gapdh*, 5′-ACCTGCCAAGTATGATGAC-3' (forward) and 5′-CTGTTGCTGTAGCCGTAT-3' (reverse). Biological reagents such as 2-mercaptoethanol (2 ME), Deferoxamine (DFO), L-Penicillamine (L-Pen), N-acetylcysteine (NAC), Trolox, and Tempol were purchased from Sigma−Aldrich, Inc. USA; AF, TRi-1, Sulfasalazine (SSZ), Ferrostatin-1 (Ferro-1), (1S,3R)-RSL3 (RSL3), Z-VAD(OH)-FMK (Z-VAD), Necrostatin-1 (NEC-1), and Chloroquine (CQ) were purchased from MedChemExpress, Inc. USA.

2.14. ^1H nuclear magnetic Resonance(^1H NMR)

A nuclear magnetic resonance spectrometer (AVANCE NEO 400MHZ, Bruker, Belgium) was used to detect the ^1H NMR spectrum of AF, TRi-1, 2 ME, NAC and L-Pen using deuterated methanol as a solvent. The ^1H NMR spectrum of the mixtures of AF and 2 ME, AF and NAC, AF and L-Pen, TRi-1 and 2 ME, TRi-1 and NAC, and TRi-1 and L-Pen were detected separately by the same method after incubation at 37 °C for 24 h.

2.15. Fluorescent staining of F-actin

2×10^4 cells/well were seeded on chamber slides in 48-well plates one day before treatments. Following treatments, the chamber slides were washed with PBS and fixed with 4% paraformaldehyde for 15 min at room temperature. The fixed cells were permeabilized with 0.3% Triton X-100 in PBS for 8 min at room temperature. Next, the permeabilized cells were incubated with 100 nM TRITC Phalloidin (Yeasen, China) for 30 min in the dark at room temperature. The cells were stained with 10 μM DAPI (Dojindo, Japan) for 10 min in the dark at room temperature. Fluorescence images were captured using a fluorescence microscope (Axio Imager Z2, Zeiss).

2.16. Micro-computed tomography (micro-CT) analyses

A microcomputed tomography (SkyScan 11772, Bruker, Belgium) was used to scan the femora of the mice. The bone mineral density (BMD), trabecular number (Tb. N), trabecular pattern factor (Tb. Pf), bone volume per tissue volume (BV/TV), and cortical thickness (Cs. Th) of the samples were analysed. The 3D images of the mouse distal femora were reconstructed using Mimics 18.0 software (Materialise, Belgium).

2.17. Bone histological analysis

A microtome (SM2500, Leica, Germany) was used to prepare 3-mm-thick sections. The calcein labeling of the distal femur was detected at 515 nm using a fluorescence microscope. The average distances between the two labels in the pictures were used to calculate the mineral apposition rate (MAR), a crucial indicator of osteoblast activity. Then, the femora were paraffin-embedded and cut into serial sections of 4 μm thickness. Hematoxylin and eosin were used to stain the trabecular bone. A TRAP staining kit (Sigma-Aldrich, USA) was used to detect TRAP-positive cells. The pictures were analysed with ImageJ software (NIH, USA).

2.18. Statistical analysis

Each experiment was conducted independently three times. The data are presented as the mean ± SD. GraphPad Prism was used for statistical analysis. Student's *t*-test was used for comparisons of two groups with normally distributed variables. One-way ANOVA with Tukey's post hoc test was used to analyse the differences between multiple groups. *P* values below 0.05 were considered statistically significant.

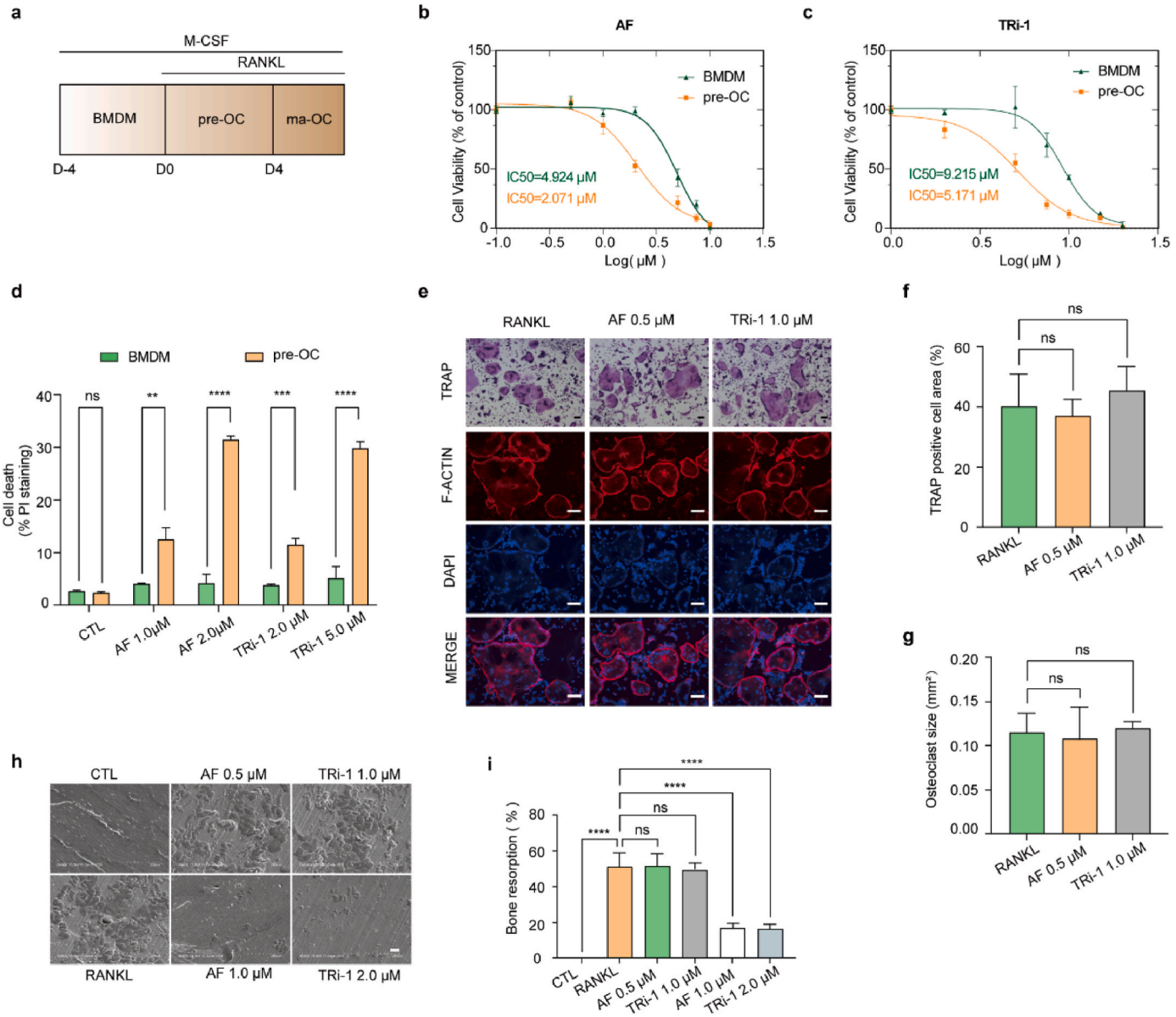

Fig. 1. Pre-OCs are more susceptible to TXNRD1 inhibitors than BMDMs, and safe doses of TXNRD1 inhibitors for pre-OCs do not impair osteoclast differentiation and bone resorption.

a, schema for osteoclast differentiation stages *in vitro*. Analysis was conducted at D0 (BMDMs), D3 (pre-OCs), and D5 (ma-OCs). (**b** to **c**), the viability of BMDMs and pre-OCs was measured after 24 h of incubation with AF (**b**) or TRi-1 (**c**). n = 3 per group. **d**, PI staining of BMDMs and pre-OCs was measured after 24 h of incubation with AF (1.0 μM, 2.0 μM) or TRi-1 (2.0 μM, 5.0 μM). n = 3 per group. (**e** to **g**), BMDMs incubated with mediums containing M-CSF, RANKL, and maximum safe doses of AF or TRi-1 for pre-OCs. TRAP staining and F-actin formation assay of ma-OCs on day 5 with quantification of TRAP-positive cell area (%) (**f**) and osteoclast size (mm^2) (**g**). Scale bar, 50 μm. n = 3 per group. (**h** to **i**), bone resorption assay was conducted on bovine cortical bone slices and the bone slices were scanned on day 7 (**h**). Scale bar, 50 μm. n = 3 per group. Bone resorption area (%) (**i**) were used to evaluate the effects of different dose of AF and TRi-1 on bone resorption capacity. All data in this figure are represented as mean ± SD. ns, no significance, **P < 0.01, ***P < 0.001, ****P < 0.0001.

3. Results

3.1. Pre-OCs are more susceptible to TXNRD1 inhibitors than BMDMs, and safe doses of TXNRD1 inhibitors for pre-OCs do not impair osteoclast differentiation and bone resorption

To assess if BMDMs and pre-OCs show different sensitivities to TXNRD1 inhibitors, we isolated BMDMs from C57BL/6 mice and induced osteoclast differentiation by M-CSF and RANKL (Fig. 1, a). To confirm that BMDMs and pre-OCs met the experimental requirements, we used flow cytometry and TRAP staining to identify primary cells. The $CD11b^{+}$ $F4/80^{+}$ cells in the BMDM samples were more than 95% (Fig. S1a). The TRAP-positive cells in the prepared pre-OC samples were more than 90% (Fig. S1, b and c). The cell viability of BMDMs and pre-OCs at different doses of AF and TRi-1 was detected by CCK-8 assays (Fig. 1b and c). The IC50 data showed that pre-OCs are more vulnerable to AF and TRi-1. PI staining showed that AF (1.0 μM, 2.0 μM) and TRi-1 (2.0 μM, 5.0 μM) selectively killed pre-OCs in a dose-dependent manner while not affecting BMDMs (Fig. 1, d, Fig. S1, d and e).

To determine whether AF and TRi-1 inhibit osteoclast differentiation

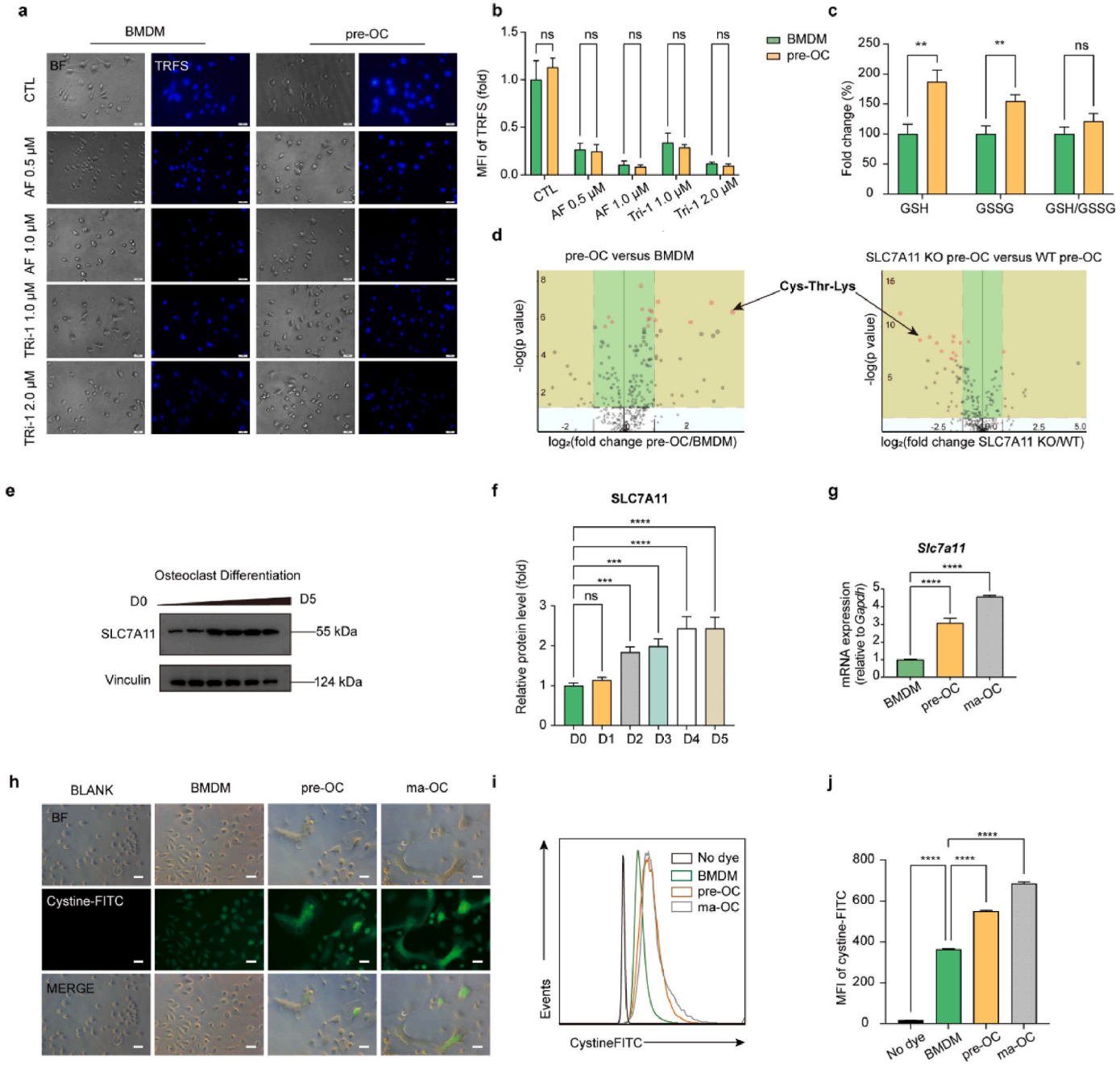

Fig. 2. SLC7A11-mediated cystine uptake and subsequent cystine reduction to cysteine in pre-OCs promote the stress of cellular disulphide metabolism. (**a** to **b**), the reductive abilities of TrxR with or without TXNRD1 inhibitors were detected by TRFS probes (**a**) and were quantified as MFI of TRFS (**b**). Scale bar, 20 μm. n = 5 per group. **c**, the relative quantitative results of intracellular GSH, GSSG, and GSH/GSSG in BMDMs and pre-OCs. n = 3 per group. **d**, the untargeted metabolome results (pre-OC versus BMDM, SLC7A11 KO pre-OC versus WT pre-OC). n = 5 per group. (**e** to **f**), western blot analysis of SLC7A11 protein levels during osteoclast differentiation. n = 3 per group. **g**, RT-qPCR analysis of *Slc7a11* in BMDMs, pre-OCs, and ma-OCs. n = 3 per group. (**h** to **j**), cystine uptake of BMDMs, pre-OCs, and ma-OCs were detected by microscopy (**h**) and flow cytometry (**i**) after being incubated with cystine-FITC probes and were quantified as MFI of cystine-FITC (**j**). Scale bar, 20 μm. n = 3 per group. All data in this figure are represented as mean ± SD. ns, no significance, $^{**}P < 0.01$, $^{***}P < 0.001$, $^{****}P < 0.0001$.

and bone resorption at safe doses for pre-OCs, we cultured BMDMs with 0.5 μM AF or 1 μM TRi-1 together with 20 ng/mL M-CSF and 50 ng/mL RANKL for five days. The TRAP staining results revealed that AF and TRi-1 at these doses did not impair the differentiation of osteoclasts. The F-actin formation assays showed no difference in F-actin formation and osteoclast size between the blank and drug-treated groups (Fig. 1e–g).

We seeded BMDMs on the surface of bovine bone slices and divided them into six groups (blank group, RANKL group, AF 0.5 μM group, AF 1.0 μM group, TRi-1 1 μM group, and TRi-1 2 μM group). After seven days of osteoclast induction, the surface morphology of the bone slices was examined by scanning electron microscopy. There were no significant differences in the area of bone resorption among the RANKL, AF 0.5 μM, and TRi-1 1.0 μM groups. The results suggested that AF and TRi-1 could not inhibit osteoclast differentiation and bone resorption at concentrations that did not impair pre-OCs. Meanwhile, the bone resorption in AF 1.0 μM and TRi-1 2 μM groups was significantly inhibited (Fig. 1h and i). These suggested that AF and TRi-1 might impair bone resorption by selectively killing pre-OC. Since previous studies reported that AF significantly reduced osteoclast numbers and effectively alleviated bone loss in OVX mice *in vivo*, combined with our experimental results, we proposed that AF and TRi-1 could treat diseases with osteoclast overactivity by selectively killing pre-OCs rather than directly inhibiting osteoclast differentiation or bone resorption.

3.2. SLC7A11-mediated cystine uptake and subsequent cystine reduction to cysteine in pre-OCs promotes the stress of cellular disulphide metabolism

To explore the underlying mechanism of the difference in sensitivity between BMDMs and pre-OCs, we first compared the inhibitory effect of TXNRDs with or without TXNRD1 inhibitors. TRFS probes displayed a fluorescence off−on change induced by TXNRDs-mediated disulphide cleavage and subsequent intramolecular cyclization to liberate the masked naphthalimide fluorophore and were used to detect the reductive abilities of TXNRDs in different groups [40]. The results showed no significant difference in the inhibitory ability of TXNRDs in BMDMs and pre-OCs, and the TXNRDs reductive abilities of the cells were inhibited to an equal degree after AF (0.5 μM, 1.0 μM) or TRi-1 (1.0 μM, 2.0 μM) treatment (Fig. 2a and b). Although TRFS-Green is not completely specific for thioredoxin reductase as recently reported [43], it can detect intracellular disulfide reduction capacity. To exclude the possibility that pre-OCs are more sensitive to TXNRD1 inhibitors due to low GSH levels or increased GSSG levels, we determined intracellular GSH and GSSG levels of BMDM and pre-OCs. Although GSH and GSSG levels were significantly higher in pre-OCs than in BMDMs, there was no significant difference in the ratio of GSH/GSSG (Fig. 2, c). These results suggested that the differences in sensitivity were not caused by the reductive activity of TXNRDs or GSH/GSSG. We proposed that differences in disulphide metabolic stress might be responsible for the differences in susceptibility to TXNRD1 inhibitors between BMDMs and pre-OCs. We compared metabolite changes in BMDMs and pre-OCs using the untargeted metabolome (Fig. S4, a and b). A total of 42 different DEMs were found in BMDMs and pre-OC metabolites, 29 of which were upregulated and 13 of which were downregulated (screening threshold: log2(FC) > 1, P < 0.05). However, we did not find disulphides among the 29 upregulated products. Since the intracellular disulphides were promptly reduced in the presence of the TXNRDs system, we searched for the disulphide-originated reduction products in the metabolites. Interestingly, Cys-Thr-Lys was significantly increased in pre-OCs compared to BMDMs (log2(FC) = 3.5375, P = 0.00000042612) (Fig. 2, d). Because SLC7A11-mediated cystine uptake is an essential source of intracellular cysteine, we hypothesized that the significant increase in Cys-Thr-Lys might be caused by increased SLC7A11-mediated cystine uptake. Intracellular disulfide stress is mainly derived from the reduction of intracellular disulfide (e.g., cystine, GSSG, etc.) and from maintaining the reactive cysteine residues in proteins [44]. As cystine is the most abundant exogenous disulphide in cells, we reasoned that increased cystine uptake may lead to increased intracellular disulphide stress in pre-OC [18,25]. To clarify the correlation between Cys-Thr-Lys and SLC7A11-mediated cystine uptake, we compared the changes in metabolites in WT pre-OCs and SLC7A11 KO pre-OCs by the untargeted metabolome. SLC7A11 KO mice were used for the preparation of SLC7A11 KO pre-OCs (Fig. S2, a and b). A total of 112 DEMs were found, of which 10 were increased and 102 were decreased (screening threshold: log2(FC) > 1, P < 0.05), and Cys-Thr-Lys was found to be significantly decreased in SLC7A11 KO pre-OCs compared to WT pre-OCs (log2(FC) = -2.3752, $P = 0.00002176$) (Fig. 2, d). These results suggested that the elevated Cys-Thr-Lys content during osteoclast differentiation correlated with SLC7A11-mediated cystine uptake.

We next examined the changes in SLC7A11 during osteoclast differentiation using RT−qPCR and Western blot, and the results showed that SLC7A11 was increased at the gene and protein levels during this process (Fig. 2e–g). We then used cystine-FITC probes to detect the cystine uptake abilities of the cells at different stages of osteoclast differentiation. The results showed that cystine uptake abilities were significantly increased in pre-OCs compared to BMDMs (Fig. 2 h-j). The above results indicated that SLC7A11-mediated cystine uptake and subsequent cystine reduction to cysteine promotes disulphide stress of pre-OCs.

3.3. NFATc1 promoted the transcription of SLC7A11 during osteoclastogenesis

According to previous reports in the literature, stimulation of primary mouse peritoneal macrophages and RAW 264.7 cells with RANKL upregulated KEAP1 and decreased the NRF2/KEAP1 ratio [45]. Numerous studies have reported that NRF2/KEAP1 plays an important role in regulating the expression of SLC7A11 [46–48]. In our study, we found that during osteoclast differentiation, SLC7A11 expression did not remain consistent with NRF2/KEAP1 but was instead temporally correlated with NFATc1, the core transcription factor of osteoclasts (Fig. 3a–c). To clarify the upstream-downstream relationship between NFATc1 and SLC7A11, we overexpressed NFATc1 in pre-OCs using a lentiviral vector and found that the expression of SLC7A11 was also upregulated (Fig. 3d–f). We used siRNA to knock down NFATc1 expression in pre-OCs, and SLC7A11 expression was also downregulated (Fig. 3g–i). To further clarify the regulatory effect of NFATc1 on SLC7A11, we performed a CUT&Tag sequencing assay in pre-OCs using an NFATc1 antibody. The heatmap of NFATc1 binding sites showed that the reads were predominantly enriched in the transcription start sites (TSSs) (Fig. 3, j). Gene ontology (GO) analysis of the genes near the peaks showed that the genes were enriched to cellular metabolic process (Fig. 3, k). We found that NFATc1 binding peaks appeared in the promoter region of SLC7A11 (NM_011990.2 and XM_006500776.3, GRCm38/mm10), as shown in the bed graph (Fig. 3, l). We designed two pairs of primers, Primers 1 for all the transcripts of SLC7A11, and Primers 2 for NM_011990.2 and XM_006500776.3. The RT−qPCR results showed that the fold change in SLC7A11 (NM_011990.2 and XM_006500776.3) expression was much higher than that in total SLC7A11 expression (Fig. S5, a and b), and the upregulated expression of NM_011990.2 and XM_006500776.3 accounted for the predominant increase in SLC7A11 expression in pre-OCs (Fig.3m). In NFATc1-overexpressing BMDMs, the fold change in SLC7A11 (NM_011990.2 and XM_006500776.3) expression was much higher than that in total SLC7A11 expression (Fig. S5, c and d), and the upregulated expression of NM_011990.2 and XM_006500776.3 accounted for the predominant increase in SLC7A11 overexpression (Fig.3n). These results suggested that NFATc1 upregulates SLC7A11 (NM_011990.2 and XM_006500776.3) expression transcriptionally during osteoclastogenesis. Then, we predicted the potential transcription factor-binding sites of NFATc1 via the Jaspar database (http://jaspar.genereg.net/), and the predicted core sequences “TTTCCA” and “TGGAAA” are listed (Fig. S3, a and b). However, no sequence containing either of these core

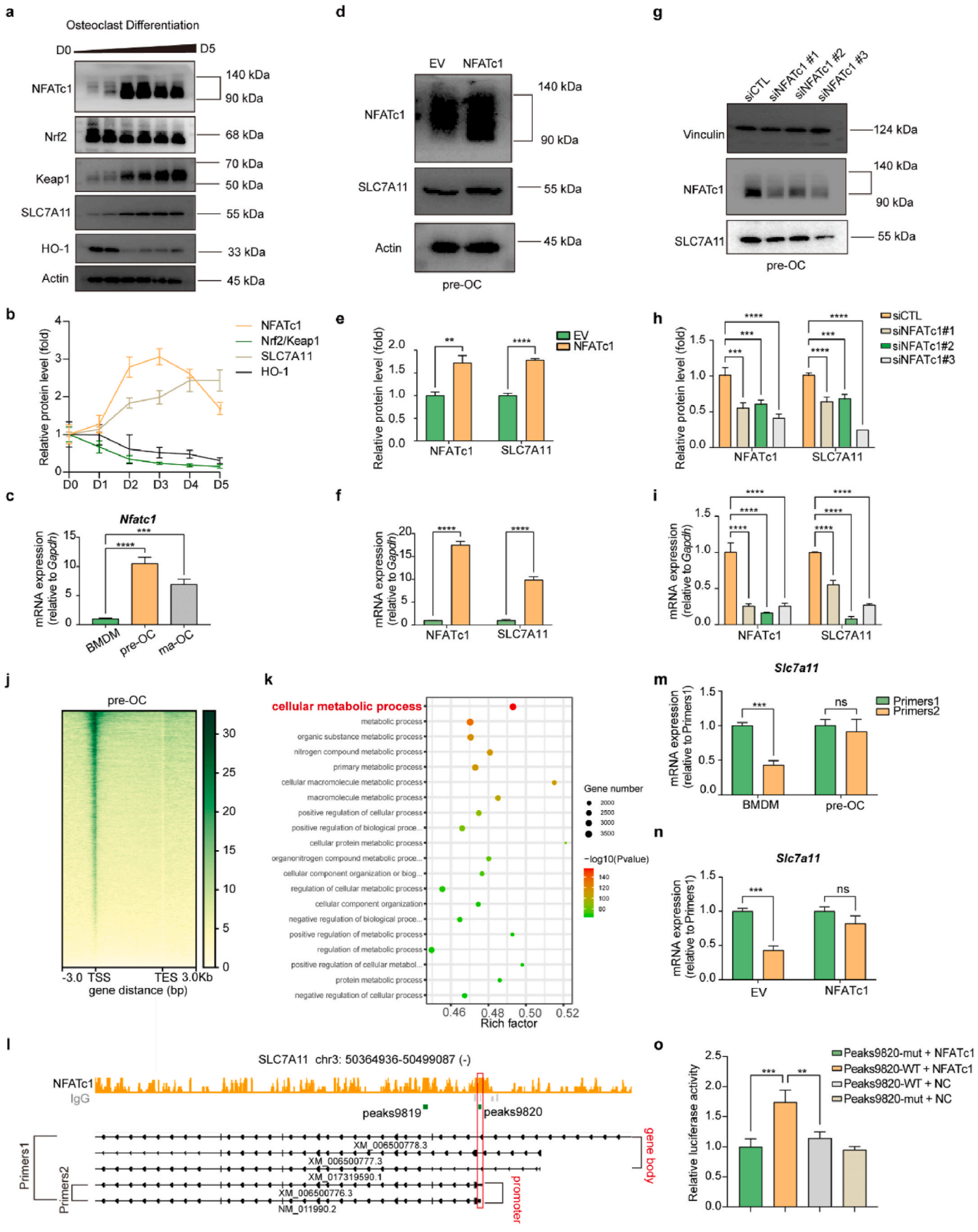

(caption on next page)

Fig. 3. NFATc1 promoted the transcription of SLC7A11 during osteoclastogenesis
(**a** and **b**), western blot analysis of NFATc1, Nrf2, Keap1, SLC7A11, and HO-1 protein levels during osteoclast differentiation. n = 3 per group. **c**, RT-qPCR analysis of *Nfatc1* in BMDMs, pre-OCs, and ma-OCs. n = 3 per group. (**d** and **e**), western blot analysis of NFATc1 and SLC7A11 protein levels in empty vector (EV) and NFATc1 overexpression pre-OCs. n = 3 per group. **f**, RT-qPCR analysis of *Nfatc1* and *Slc7a11* in empty vector (EV) and NFATc1 overexpression pre-OCs. n = 3 per group. (**g** and **h**), western blot analysis of NFATc1 and SLC7A11 protein levels in siControl (siCTL) and siNFATc1 pre-OCs. n = 3 per group. **i**, RT-qPCR analysis of *Nfatc1* and *Slc7a11* in siControl (siCTL) and siNFATc1 pre-OCs. n = 3 per group. **j**, heatmap for the distribution of NFATc1 binding sites detected by CUT&Tag assay in pre-OCs. TSS transcription, start site, TES, transcription end site. **k**, Gene Ontology (GO) analysis of the genes near the peaks. **l**, genomic binding pattern of the *Slc7a11* locus showing the NFATc1-binding locations. **m**, RT-qPCR analysis using Primers 1 and Primers 2 of *Slc7a11* in BMDMs and pre-OCs. n = 3 per group. **n**, RT-qPCR analysis using Primers 1 and Primers 2 of *Slc7a11* in EV and NFATc1 overexpression in BMDMs. n = 3 per group. **o**, Dual-Luciferase reporter assay conducted in MC3T3-E1 cell line. n = 3 per group. All data in this figure are represented as mean ± SD. ns, no significance, $^{**}P < 0.01$, $^{***}P < 0.001$, $^{****}P < 0.0001$.

sequences was found in peak 9820. A previous study reported that NFATC1 could combine with "ATTTCC" to play a transcriptional regulatory role [49]. Considering the predicted sequence "TTTCCA" and the reported sequence "ATTTCC", we speculated that "TTTC" in peak 9820 would be the core sequence of NFATc1. A luciferase reporter assay was used to further confirm the binding site of NFATc1 in SLC7A11 regulation. It was shown that NFATc1 promoted the SLC7A11 transcription, while transcription was significantly down-regulated after we mutated the binding site from 5′-TTTC-3′ to 5′-CCCT-3' (Fig. 3, o). The total of these results indicated that NFATc1 promoted the transcription of SLC7A11 by binding the sequence "TTTC" located in the promoter region of NM_011990.2 and XM_006500776.3.

3.4. The ferroptosis inhibitors (DFO, Ferro-1), the ROS scavengers (Trolox, Tempol), the apoptosis inhibitor (Z-VAD), the necroptosis inhibitor (Nec-1), or the autophagy inhibitor (CQ) cannot rescue TXNRD1 inhibitor-induced cell death in pre-OCs

Cystine starvation or pharmacological SLC7A11 inhibition induces ferroptotic cell death. Cystine deprivation leads to a shortage of cysteine and impaired GSH synthesis. The subsequent increase in intracellular lipid peroxidation leads to ferroptosis. Previous studies reported that the TXNRD1 inhibitor AF blocked cystine reduction, impaired GSH synthesis, and induced ferroptosis in cancer cells [29]. Our study indicated that TXNRD1 inhibitor-induced cell death in pre-OCs differed from ferroptosis. We used Liperfluo probes to evaluate cellular lipid peroxidation, and no significant changes were found in pre-OCs or BMDMs after TXNRD1 inhibitor treatments (Fig. 4a and b). We examined the difference in sensitivity of BMDMs and pre-OCs to the ferroptosis inducer RSL3, and the results showed that pre-OCs were significantly more resistant to RSL3-induced ferroptosis than BMDMs (Fig. 4, c). Furthermore, ferroptosis inhibitors [Ferrostatin-1 (Ferro-1) and iron chelator deferoxamine (DFO)] could not rescue the cell death induced by TXNRD1 inhibitors in pre-OCs (Fig. 4d and e). Overall, these results showed that cell death in this context was different from ferroptosis.

The finding that the ROS level in BMDMs was significantly elevated after RANKL stimulation is acknowledged [50]. Moreover, our study, together with previous research [51], suggested that TXNRD1 inhibitors increased intracellular ROS. As pre-OCs have higher basal ROS levels than BMDMs, higher ROS levels in pre-OCs after TXNRD1 inhibitor interventions might render pre-OCs more sensitive to TXNRD1 inhibitors (Fig. 4f and g). Unexpectedly, although ROS scavengers (Trolox and Tempol) could inhibit intracellular ROS levels (Fig. 4i and j), they could not rescue cell death in this case (Fig. 4, h). These results indicated that cell death in this context was not caused by ROS per se.

To further investigate the type of cell death induced by 2 μM AF or 5 μM TRi-1 in pre-OCs, we used the apoptosis inhibitor Z-VAD, the necrotrophic apoptosis inhibitor Nec-1 and the autophagy inhibitor CQ to rescue cell death. The results showed that neither Z-VAD, NEC-1 nor CQ were effective in rescuing this type of cell death (Fig. 4, k and i).

3.5. Treatments that prevent disulphide accumulation or pharmacological SLC7A11 inhibition rescued the cell death induced by TXNRD1 inhibitors in pre-OCs

The HPLC-MS/MS results showed that the intracellular cystine levels of pre-OCs were significantly higher than those of BMDMs after treatment with TXNRD1 inhibitors (Fig. 5, a). N-acetylcysteine (NAC), a chemically stable cysteine supplement, inhibits intracellular ROS levels by promoting GSH synthesis on the one hand and diminishes intracellular disulphide accumulation through disulphide exchange on the other hand. Our results suggested that NAC obviously reduced the cellular cystine concentration and rescued the cell death caused by TXNRD1 inhibitors in pre-OCs (Fig. 5b and c).

L-Penicillamine (L-Pen) is widely used clinically to treat cystinuria, a disease caused by cystine accumulation in the bladder. This treatment displaces the disulphide bond in cystine, thereby reducing the cystine to a soluble substance (Cys-Cys + penicillamine → Cys + Cys-penicillamine). Although L-penicillamine cannot be metabolized to cysteine and promote GSH synthesis, similar to NAC, it reduced intracellular cystine accumulation and rescued cell death caused by TXNRD1 inhibitors in pre-OCs (Fig. 5d and e).

Moreover, 2-mercaptoethanol (2 ME) is often used to disrupt the disulphide bonds that hold the protein structure and makes it convenient for protein analysis. This molecule was used in this study to reduce the disulphide accumulated in pre-OCs. The results showed that 2 ME reduced intracellular cystine content and rescued cell death in this context (Fig. 5f and g).

To exclude the possibility that these reductants (NAC, 2 ME, L-Pen) rescued the phenotype by reacting directly with AF or TRi-1, we examined drug interactions using ^{1}H NMR and the results suggested that no significant interactions occurred between the reducing molecules and the TXNRD1 inhibitors when incubated in deuterated methanol solution at 37 °C for 24 h (Fig. S7, a to k).

Although the three kinds of disulphide-reducing agents above were proven to be effective in reducing intracellular cystine accumulation and rescuing TXNRD1-induced cell death in pre-OCs, all of these disulphide reducers are not cystine-specific and can reduce other molecules such as GSSG or proteins. Therefore, we used sulfasalazine (SSZ) to investigate the effect of blocking cystine uptake rather than reducing intracellular disulphides on TXNRD1 inhibitor-induced cell death. The HPLC–MS/MS and CCK-8 results showed that SSZ effectively reduced intracellular cystine accumulation and rescued TXNRD1-induced cell death (Fig. 5h and i).

3.6. NFATc1 knockdown in pre-OCs reduced cell sensitivity to TXNRD1 inhibitors, SLC7A11 knockout abolished the difference in sensitivity of BMDMs and pre-OCs to TXNRD1 inhibitors, and overexpression of SLC7A11 or NFATc1 in BMDMs increased cell sensitivity to TXNRD1 inhibitors

To further clarify that NFATc1-regulated SLC7A11-mediated cystine uptake renders pre-OCs more susceptible to TXNRD1 inhibitors, we knocked down NFATc1 in pre-OCs and found that NFATc1 knockdown significantly reduced intracellular cystine levels after TXNRD1 inhibitor treatments and decreased the sensitivity of pre-OCs to TXNRD1

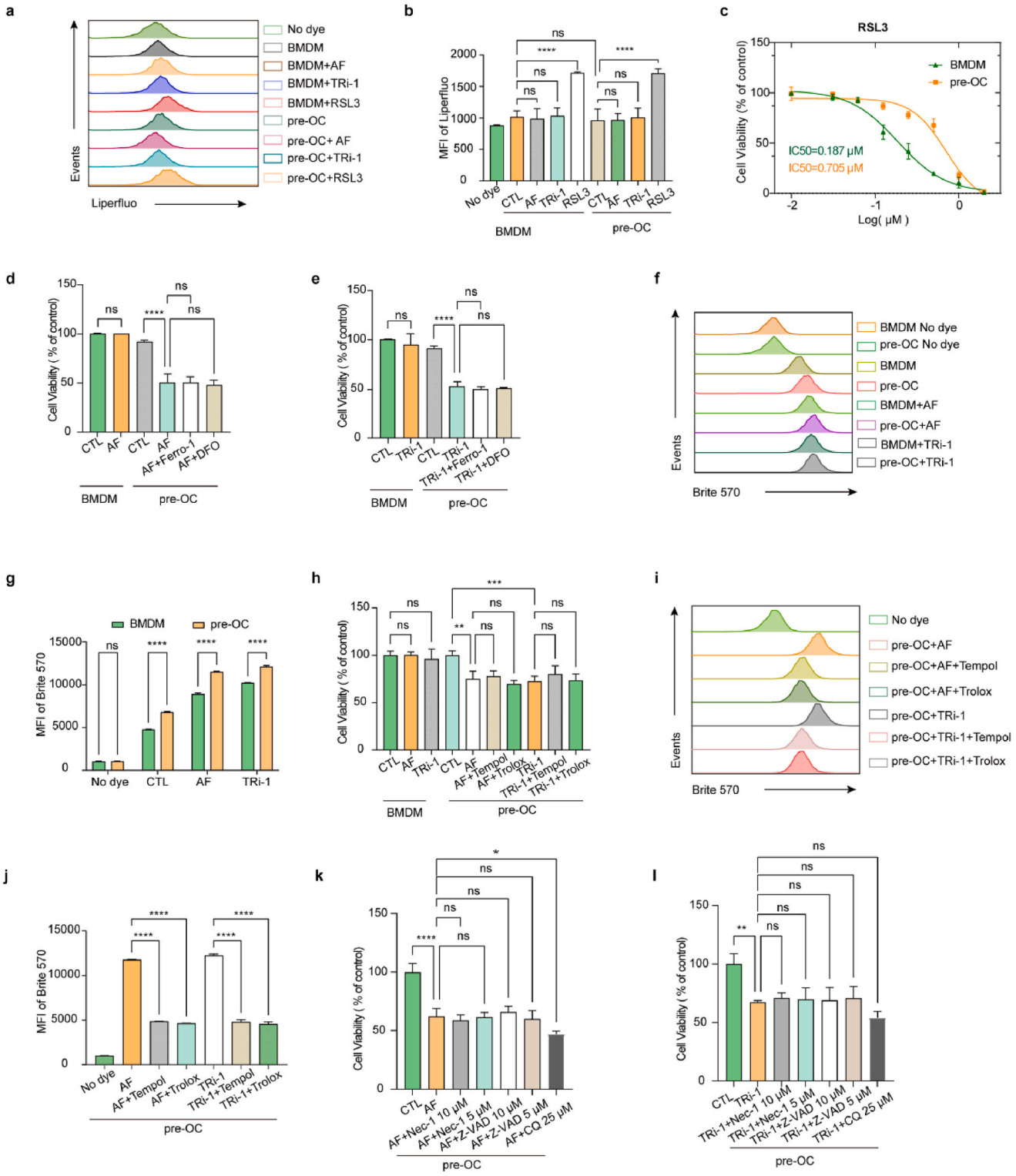

Fig. 4. The ferroptosis inhibitors (DFO, Ferro-1), the ROS scavengers (Trolox, Tempol), the apoptosis inhibitor (Z-VAD), the necroptosis inhibitor (Nec-1), or the autophagy inhibitor (CQ) cannot rescue TXNRD1 inhibitor-induced cell death in pre-OCs

(**a** and **b**), lipid peroxidation was detected by Liperfluo using flow cytometry. n = 3 per group. **c**, the viability of BMDMs and pre-OCs was measured after 24 h of incubation with RSL3. n = 3 per group. **d**, the viability of BMDMs and pre-OCs was measured after 24 h of incubation with a medium containing 2 μM AF with or without 2 μM Ferrostantin-1 or 50 μM DFO. n = 3 per group. **e**, the viability of BMDMs and pre-OCs was measured after 24 h of incubation with a medium containing 5 μM TRi-1 with or without 2 μM Ferrostantin-1 or 50 μM DFO. n = 3 per group. (**f** and **g**) ROS levels were detected by Brite 570 using flow cytometry. n = 3 per group. **h**, the viability of BMDMs and pre-OCs was measured after 5 h of incubation with a medium containing 2 μM AF or 5 μM TRi-1with or without 100 μM Trolox or 25 μM Tempol. n = 3 per group. (**i** and **j**) ROS levels were detected by Brite 570 using flow cytometry. n = 3 per group. (**k** and **l**) the viability of pre-OCs was measured after 12 h of incubation with a medium containing 2 μM AF or 5 μM TRi-1with or without Nec-1 (5 μM, 10 μM), Z-VAD (5 μM, 10 μM), or CQ (25 μM). n = 3 per group. All data in this figure are represented as mean ± SD. ns, no significance, *P < 0.01, **P < 0.01, ***P < 0.001, ****P < 0.0001.

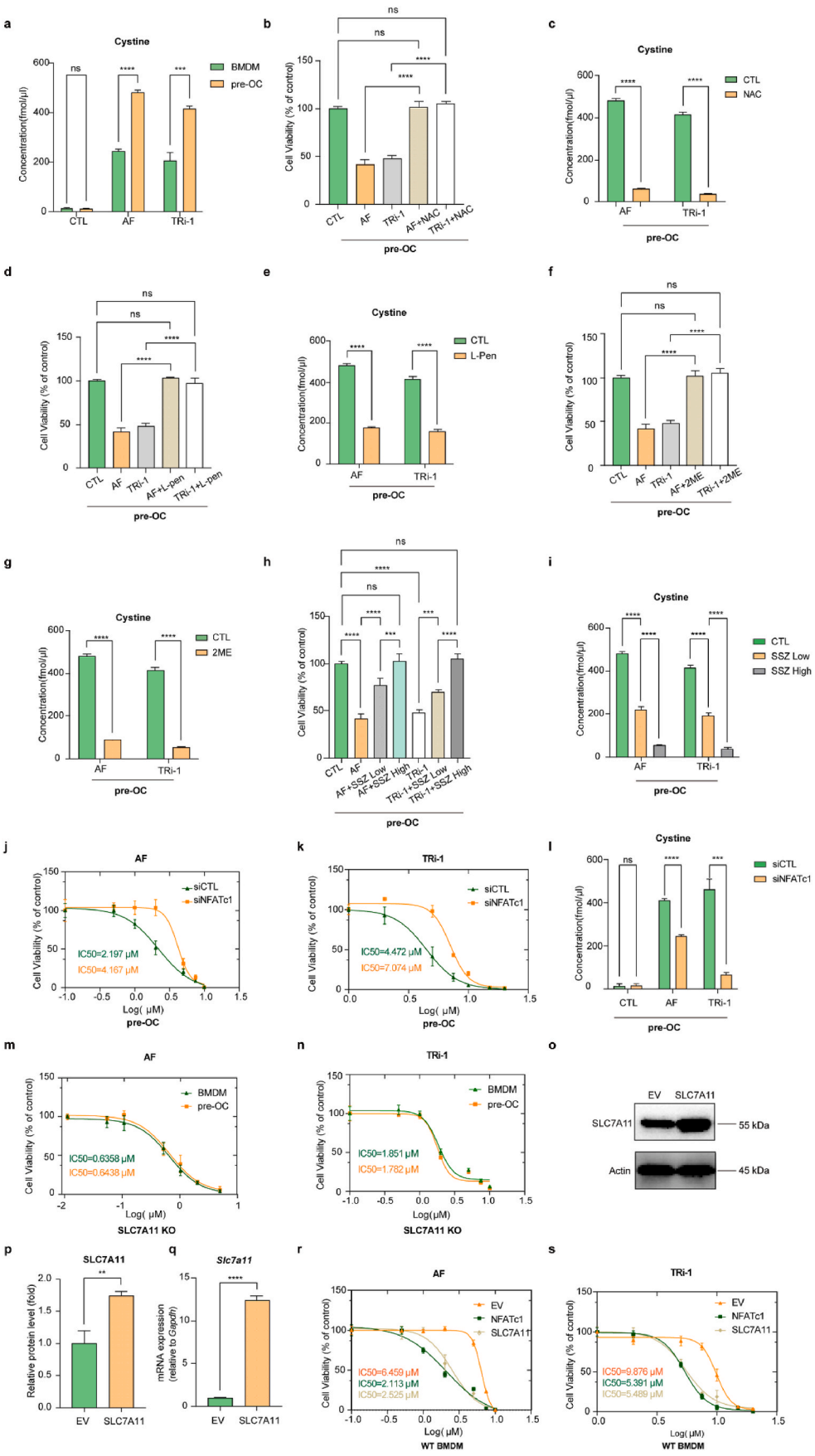

Fig. 5. Treatments that prevent disulphide accumulation or pharmacological SLC7A11 inhibition rescued the cell death induced by TXNRD1 inhibitors in pre-OCs. NFATc1 knockdown in pre-OCs attenuated TXNRD1 inhibitor-induced cystine accumulation and decreased the sensitivity to TXNRD1 inhibitors. SLC7A11 knockout eliminated the difference in sensitivity of BMDMs and pre-OCs to TXNRD1 inhibitors, and overexpression of SLC7A11 or NFATc1 in BMDMs increased cell sensitivity to TXNRD1 inhibitors

a, the HPLC-MS/MS results of intracellular cystine concentrations in BMDMs, BMDMs treated with TXNRD1 inhibitors, pre-OCs, and pre-OCs treated with TXNRD1 inhibitors. n = 3 per group. **b**, the viability of pre-OCs was measured after 24 h of incubation with a medium containing 2 μM AF or 5 μM TRi-1 with or without 5 mM NAC. n = 3 per group. **c**, the HPLC-MS/MS results of intracellular cystine concentrations in pre-OCs treated with TXNRD1 inhibitors and pre-OCs treated with both TXNRD1 inhibitors and NAC. n = 3 per group. **d**, the viability of BMDMs and pre-OCs was measured after 24 h of incubation with a medium containing 2 μM AF or 5 μM TRi-1 with or without 500 μM L-Penicillamine (L-Pen). n = 3 per group. **e**, the HPLC-MS/MS results of intracellular cystine concentrations in pre-OCs treated with TXNRD1 inhibitors and pre-OCs treated with both TXNRD1 inhibitors and L-pen. n = 3 per group. **f**, the viability of BMDMs and pre-OCs was measured after 24 h of incubation with a medium containing 2 μM AF or 5 μM TRi-1 with or without 2 mM 2-Mercaptoethanol (2 ME). n = 3 per group. **g**, The HPLC-MS/MS results of intracellular cystine concentrations in pre-OCs treated with TXNRD1 inhibitors and pre-OCs treated with both TXNRD1 inhibitors and 2 ME. n = 3 per group. **h**, the viability of BMDMs and pre-OCs was measured after 24 h of incubation with medium containing 2 μM AF or 5 μM TRi-1 with or without Sulfasalazine (SSZ) (low dose 100 μM, high dose 400 μM). n = 3 per group. **i**, the HPLC-MS/MS results of intracellular cystine concentrations in pre-OCs treated with TXNRD1 inhibitors and pre-OCs treated with both TXNRD1 inhibitors and SSZ. n = 3 per group. (**j** and **k**), the viability of siCTL and siNFATc1 pre-OCs was measured after 24 h of incubation with AF (**j**) or TRi-1 (**k**). n = 3 per group. **l**, The HPLC-MS/MS results of intracellular cystine concentrations in siCTL and siNFATc1 pre-OCs treated with TXNRD1 inhibitors, n = 3 per group (**m** and **n**), the viability of SLC7A11 KO BMDMs and pre-OCs was measured after 24 h of incubation with AF (**m**) or TRi-1 (**n**). n = 3 per group (**o** and **p**), western blot analysis of SLC7A11 protein levels in EV and SLC7A11 overexpression BMDMs. n = 3 per group. **q**, RT-qPCR analysis of *Slc7a11* in EV and SLC7A11 overexpression BMDMs. n = 3 per group. (**r** and **s**), the viability of EV, NFATc1 overexpression, and SLC7A11 overexpression BMDMs was measured after 24 h of incubation with AF (**r**) or TRi-1 (**s**). n = 3 per group. All data in this figure are represented as mean

± SD. ns, no significance, **P < 0.01, ***P < 0.001, ****P < 0.0001.

inhibitors (Fig. 5, j to l).

To further clarify that SLC7A11-mediated cystine uptake leads to differences in BMDMs and pre-OCs to TXNRD1 inhibitors, we extracted BMDMs from SLC7A11$^{-/-}$ mice and compared the differences in the sensitivity of SLC7A11$^{-/-}$ BMDMs and pre-OCs to AF and TRi-1. We found that although SLC7A11$^{-/-}$ BMDM and pre-OCs were more sensitive to AF and TRi-1 than WT, the difference in sensitivity between BMDM and pre-OCs was abolished (Fig. 5, m and n). A previous study revealed that mammalian thioredoxin and glutathione systems were able to provide electrons to each other and serve as a backup system for each other [21]. The deleted SLC7A11-mediated cystine uptake impaired GSH synthesis and resulted in glutathione system breakdown. Under this condition, the thioredoxin system functions as the predominant antioxidant system to maintain intracellular redox homeostasis, and inhibition of TXNRD1 might lead to oxidative stress-induced cell death.

We used lentivirus to overexpress SLC7A11 and NFATc1 in BMDMs. Overexpression efficiencies were detected using RT–qPCR and Western blot (Fig. 3d–f, Fig. 5, o to q). The results showed that overexpression of SLC7A11 or NFATc1 increased the susceptibility of BMDMs to AF and TRi-1 compared to controls (Fig. 5, r and s).

To confirm that the phenotypes were due to inhibition of TXNRD1, we knocked down TXNRD1 in BMDMs and found that TXNRD1 knockdown significantly increased the sensitivity of BMDMs to TXNRD1 inhibitors (Fig. S6, d to h).

We examined the mRNA and protein levels of BMDMs and pre-OCs after treatment with 0.5 μM AF or 1 μM TRi-1 for 24 h. The results showed that although the mRNA levels of SLC7A11 in BMDMs and pre-OCs changed 24 h after the treatments, no significant changes were observed in the protein levels (Fig. S6, a to c). The results suggested that the rate of cystine uptake in BMDMs and pre-OCs did not change significantly 24 h after the treatments. Therefore, we can exclude the possibility that the change in cystine uptake rate after the TXNRD1 inhibitor treatments affects the validity of our results.

3.7. TXNRD1 inhibition induced F-actin contraction in pre-OCs

Recent research has shown that actin cytoskeleton proteins are particularly susceptible to disulfide stress caused by excessive accumulation of intracellular cystine, and the aberrant disulfide bonds between actin cytoskeleton proteins lead to cell death. The researchers named this type of cell death disulfidptosis and identified cystine accumulation

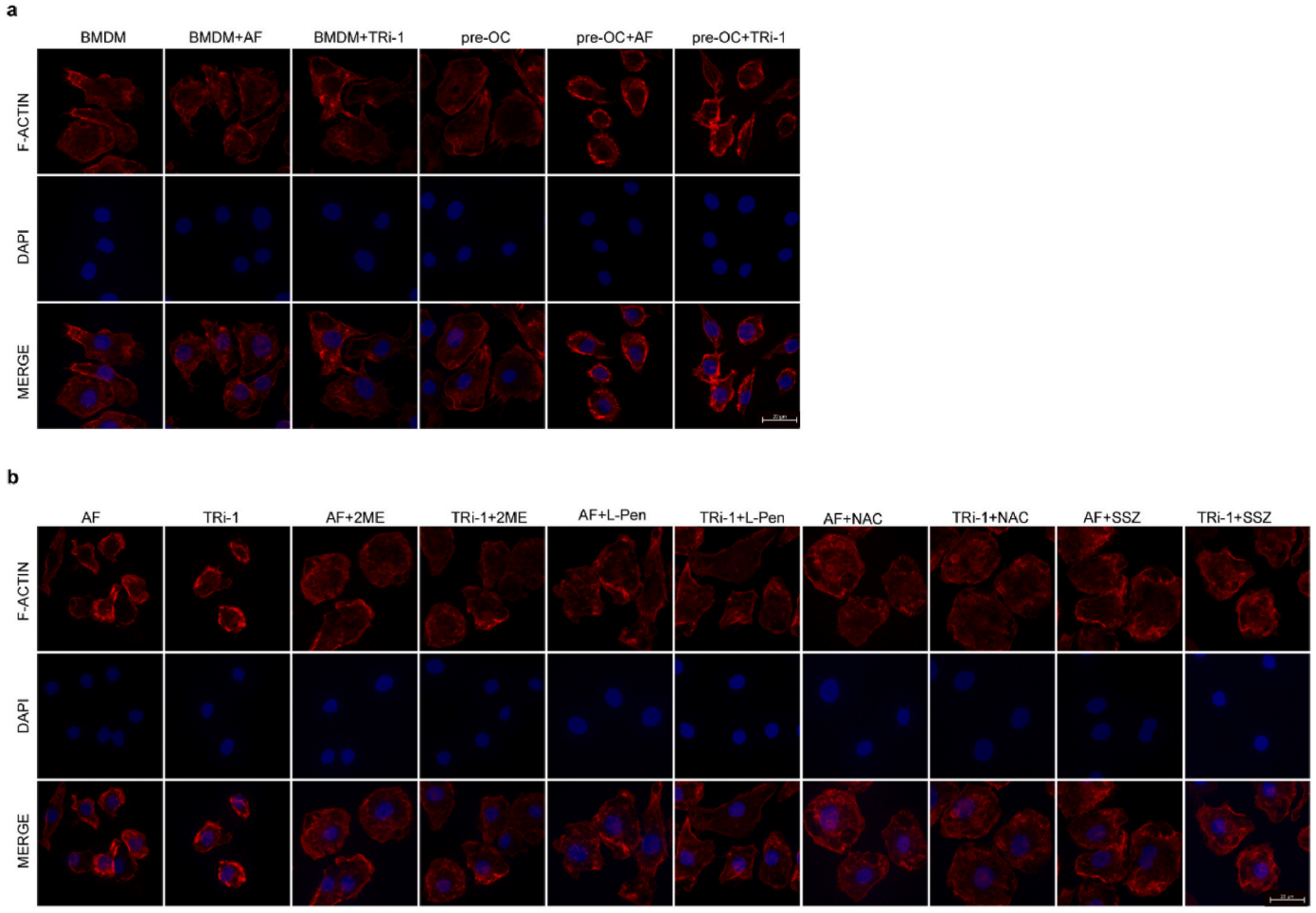

Fig. 6. F-actin contracted during TXNRD1 inhibitor-induced cell death

a, Rhodamine labelled phalloidin staining of F-actin and DAPI staining of nuclei in BMDMs and pre-OCs treated with or without AF (2 μM) or TRi-1 (5 μM) for 3h. Scale bar, 20 μm

b, F-actin and DAPI staining of pre-OCs treated with AF (2 μM) or TRi-1 (5 μM) with or without 2 ME (2 mM), L-Pen (500 μM), NAC (5 mM), and SSZ (400 μM). Scale bar, 20 μm.

and F-actin contraction as the two hallmarks of this type of death [25]. To exclude the effect of cell death on cell morphology, we performed F-actin staining before obvious cell death induction (Fig. S6 i). The F-actin staining results showed that 2 μM AF or 5 μM TRi-1 significantly contracted the F-actin of pre-OCs, whereas it had no significant effect on the F-actin morphology of BMDMs (Fig. 6 a). Treatments that prevented disulfide accumulation or pharmacological SLC7A11 inhibition rescued F-actin contraction induced by TXNRD1 inhibitors (Fig. 6 b).

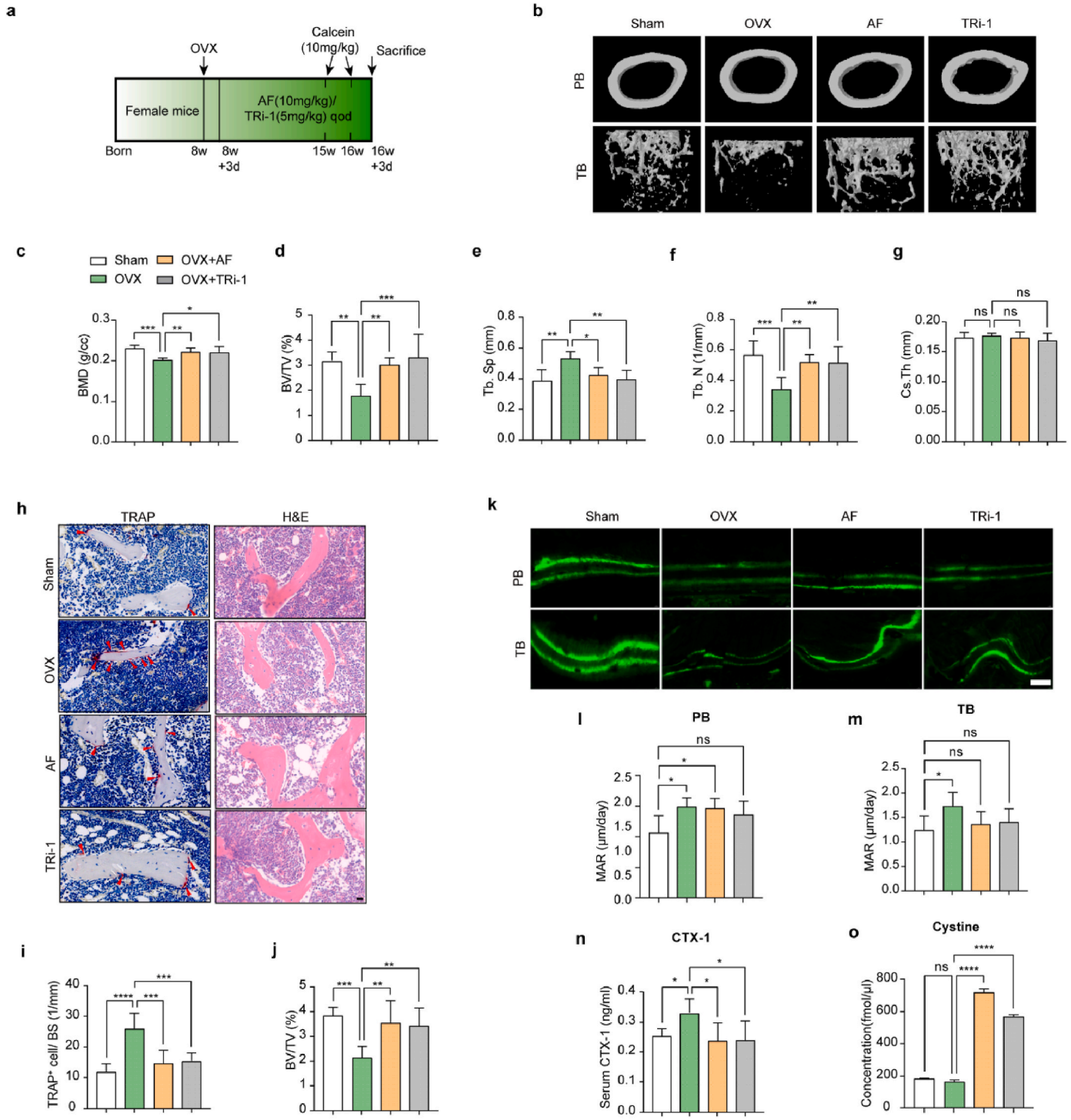

Fig. 7. TXNRD1 inhibitors increased cystine content in mouse femurs, reduced TRAP-positive cells, and attenuated bone loss in OVX mice
a, schema for *in vivo* experiments. **b**, representative micro-CT images of femora [periosteal bone (PB) and trabecular bone (TB)] of sham, OVX, and drug-treated mice. n = 6 per group. (**c** to **g**), quantitative micro-CT of BMD, BV/TV, Tb. Sp, Tb. N, and Cs. Th. n = 6 per group. **h**, TRAP staining and H&E staining, the trabecular bone (TB). Arrow, $TRAP^+$ cells; BM, bone marrow. Scale bars, 20 μm. n = 6 per group. **i**, quantification of $TRAP^+$ cells/bone surface according to TRAP staining images. n = 6 per group. **j**, quantification of BV/TV according to H&E staining images, n = 6 per group. **k**, images of calcein double labeling of PB and TB. Scale bar, 20 μm. (**l** and **m**), quantification of mineral apposition rate (MAR) in calcein double labeling. n = 6 per group. **n**, serum CTX-1 levels. n = 6 per group. **o**, tibia cystine concentrations. n = 3 per group. All data in this figure are represented as mean ± SD. ns, no significance, *P < 0.05, **P < 0.01, ***P < 0.001, ****P < 0.0001.

3.8. TXNRD1 inhibitors increased cystine content in mouse femora, reduced TRAP-positive cells, and attenuated bone loss in OVX mice

To further determine the protective effects of TXNRD1 inhibitors *in vivo*, we intraperitoneally injected AF (10 mg/kg) or TRi-1 (5 mg/kg) into OVX mice every two days. We recorded the body weights of the mice every week (Fig. S8 b). After 8 weeks, we used micro-CT to scan the distal femora of the mice, and the relevant parameters [bone mineral density (BMD), bone volume per tissue volume (BV/TV), trabecular separation (Tb. Sp), number of trabeculae (Tb. N), and cortical thickness (Cs.Th)] showed that bone loss was significantly attenuated after treatment with AF (10 mg/kg) or TRi-1 (5 mg/kg) (Fig. 7b–g). The results of H&E staining showed that there were more bone trabeculae in the AF or TRi-1 group than in the OVX group. TRAP staining results showed fewer TRAP-positive cells in the AF group and TRi-1 group than in the OVX group (Fig. 7h–j). The results of calcein double labeling for measuring femoral bone formation showed that the mineral apposition rate (MAR), compared to the sham groups, was significantly higher in the OVX group and did not change significantly in the drug-treated groups (Fig. 7, k to m). The results indicated that TXNRD1 inhibitors significantly downregulated bone turnover rate and did not significantly impair bone mineralization deposition *in vivo*. The ELISA results of C-telopeptide of type I collagen (CTX-1) showed that bone resorption was inhibited in the drug-treated groups (Fig. 7, n). The HPLC−MS/MS results showed that the cystine contents of mouse tibiae were significantly increased in the drug-treated groups compared to the sham group and the OVX groups (Fig. 7, o). Combined with the results of the *in vitro* experiments, we proposed that cystine accumulation in pre-OCs accounted for the elevated cystine levels in bone tissue. The uteruses of the mice in the OVX and drug-treated groups were smaller than those of the sham group (Fig. S8a). H&E staining of organs after sacrifice indicated that intraperitoneal AF (10 mg/kg) or TRi-1 (5 mg/kg) injection during this process had no significant toxic to these organs in OVX mice (Fig. S8 c).

4. Discussion

In this study, we demonstrated that during RANKL-mediated osteoclastogenesis, pre-OCs are more susceptible to TXNRD1 inhibitors than BMDMs. Untargeted metabolomic analysis revealed that Cys-Thr-Lys was significantly increased in pre-OCs. Excessive cystine uptake during osteoclast differentiation might lead to an increase in Cys-Thr-Lys and add metabolic stress of disulphides in pre-OCs, thus rendering pre-OCs more susceptible to TXNRD1 inhibitors. Further studies revealed that NFATc1 upregulates SLC7A11 through transcriptional regulation during osteoclast differentiation, resulting in increased cystine uptake of pre-OCs. During TXNRD1 inhibition, the rate of intracellular disulfide reduction is significantly reduced. The accumulation of cystine increased cellular disulphide stress, formatting the aberrant disulphide bonds between actin cytoskeleton proteins and leading to cell death. We further demonstrated that the SLC7A11 inhibitor SSZ and treatments that prevent cystine accumulation could rescue this type of cell death, whereas the ferroptosis inhibitors (DFO, Ferro-1), the ROS scavengers (Trolox, Tempol), the apoptosis inhibitor (Z-VAD), the necroptosis inhibitor (Nec-1), or the autophagy inhibitor (CQ) could not. *In vivo* studies showed that TXNRD1 inhibitors increased bone cystine content, reduced the number of osteoclasts in bone tissue, and alleviated bone loss in OVX mice.

In previous studies, we have identified a number of small molecule drugs that could alleviate OVX-induced bone loss in mice by preventing pre-OC fusion or inhibiting osteoclast differentiation [39,52–54]. In the course of these studies, we found that the susceptibility of cells to certain drugs changes during osteoclast differentiation. We found that pre-OCs were more sensitive to TXNRD1 inhibitors and selected a safe dose based on the CCK-8 results of pre-OCs. Interestingly, TXNRD1 inhibitors have no significant effect on osteoclast differentiation and resorption at such doses. However, AF was approved by the FDA in 1985 as a treatment for rheumatoid arthritis and has been proven to alleviate bone destruction. Previous studies showed that AF reduced the number of osteoclasts and alleviated bone loss in OVX mice [55,56]. Accordingly, we deduced that TXNRD1 inhibitors do not work by inhibiting osteoclast differentiation but by selectively killing pre-OCs. As the Trx system's reductive capacity and GSH/GSSG ratio did not change significantly in BMDMs and pre-OCs, we speculated that the changes in disulphide metabolism might cause the difference in sensitivity. Interestingly, the results of the untargeted metabolome did not reveal significant changes in disulphide levels, but the levels of the cysteine-containing tripeptide Cys-Thr-Lys were significantly increased. Since the intracellular conversion of cystine to cysteine is an immediate process, more cystine uptake may improve intracellular cysteine and increase the content of Cys-Thr-Lys. Previous research reported that NRF2/KEAP1 is downregulated during osteoclast differentiation [45]. Meanwhile, a number of studies have reported that NRF2/KEAP1 play a key role in upregulating SLC7A11 [46–48]. However, our study found that, unlike other NRF2-regulated genes, SLC7A11 expression was increased during osteoclast differentiation. NFATc1 is a crucial transcription factor in osteoclast differentiation and has recently been reported to be involved in the metabolic reprogramming of many immune cells [57]. We found a temporal correlation between NFATc1 and SLC7A11 expression. Knockdown or overexpression of NFATc1 led to increased and decreased expression of SLC7A11. The CUT&Tag results showed that NFATc1 binds to the promoter region of *slc7a11*. However, the reported core sequence of NFATc1 was not found among the NFATc1-binding sequences. A previous study showed that NFATc1 could bind 5′-ATTTCC-3′ to play a transcriptional role, and 5′-TTTC-3′ was found in peak 9820. Accordingly, we speculated that 5′-TTTC-3′ in the peak might be the core sequence of NFATc1. Subsequent dual-luciferase reporter assays verified our hypothesis. In this study, we first reported the transcriptional regulation of SLC7A11 by NFATc1 and identified a new core sequence of NFATc1. Previous studies have shown that the activation of many immune cells is highly dependent on SLC7A11-mediated cystine uptake, as cystine is critical for maintaining intracellular redox homeostasis [58–60]. However, its regulatory mechanism still needs to be clarified. NFATc1 is also essential for the differentiation of these cells, but its regulation of *slc7a1*1 has not been reported. Our study coupled the immune cell core transcription factor NFATc1 and the cystine transport system, providing new evidence that NFATc1 mediates the metabolic reprogramming of immune cells and regulates cellular redox homeostasis.

AF has recently been widely reported as an antitumor agent due to its inhibitory effect on TXNRD1 [30,36,61]. However, as a drug approved by the FDA for the treatment of rheumatoid arthritis, its inhibition of TXNRD1 has not been investigated in related diseases. Our study demonstrated that AF selectively kills pre-OCs by inhibiting TXNRD1 to alleviate osteoclast-related disease. TRi-1, a specific TXNRD1 inhibitor, was used to validate this finding. Previous studies have shown that AF is an effective ferroptosis inducer [29]. For human hepatocytes, low concentrations of AF induced cellular ferroptosis by upregulating hepcidin expression, and high concentrations of AF led to ferroptosis by depleting cysteine through TXNRD1 inhibition [29]. We found that cellular lipid peroxidation levels in pre-OCs did not improve after AF treatment, and cell death could not be rescued by ferroptosis inhibitors. Therefore, we concluded that this cell death phenotype is different from ferroptosis. Interestingly, we examined the difference in sensitivity of BMDMs and pre-OCs to the canonical ferroptosis inducer RSL3, and the results suggest that pre-OCs resist RSL3-induced ferroptosis, which contrasts with the results that pre-OCs are more sensitive to apoptosis and TXNRD1 inhibitors [62]. Since cells with high expression of SLC7A11 or low expression of HO-1 tended to be more resistant to ferroptosis, we inferred that increased SLC7A11 levels and decreased HO-1 levels in pre-OCs led to the resistance [63,64]To clarify our findings, further studies are needed in the future. AF has been reported to significantly

increase intracellular ROS levels, leading to impaired oxidative stress [51]. Activation of ROS is critical for osteoclast differentiation, and the ROS levels in pre-OCs are higher than those in BMDMs. This difference in ROS levels may account for the difference in sensitivity to TXNRD1 inhibitors. The ROS scavengers Trolox and Tempol were used to decrease intracellular ROS levels but could not rescue cell death. These results suggested that ROS per se did not drive cell death in this context. A previous article reported that cells with high SLC7A11 expression are more sensitive to NADPH depletion because pumped-in cysteine cannot be reduced to cysteine in this case and induces cell death [18]. Our experiments revealed that the disulphide reducer 2 ME and thiol compounds such as NAC and penicillamine rescued the cell death induced by TXNRD1 inhibition. This evidence suggests that cell death in this context is caused by disulphide accumulation. We further pharmacologically inhibited SLC7A11, and cell death could be rescued, suggesting that cystine uptake is the main source of intracellular disulphide stress. The latest study showed that actin cytoskeleton proteins are particularly susceptible to disulfide stress [25]. Our research showed that increased cystine uptake during TXNRD1 inhibition in pre-OCs increases intracellular disulfide stress, leading to cystine accumulation and F-actin contraction, resulting in disulfidptosis. Together, our findings suggest that TXNRD1 inhibitors induced pre-OC death is disulfidptosis and complement the pharmacological mechanisms of TXNRD1 inhibitors.

In this research, we compared the susceptibility of BMDMs and pre-OCs to TXNRD1 inhibitors but did not explore the drug toxicity on other SLC7A11^{high} cells. Although *in vivo* experiments showed that AF and TRi-1 had no significant toxic effects on mouse viscera and did not affect osteoblast differentiation at therapeutic concentrations, the drugs could damage other SLC7A11^{high} cells. A targeted drug delivery system, such as using liposome-encapsulated drugs to target the cells, may prevent such inadvertent damage. In addition, pre-OCs play a vital role in promoting angiogenesis and fracture healing. Pre-OCs secrete cytokines such as platelet-derived growth factor beta polypeptide b (PDGF-BB) to promote the growth of H-type blood vessels and accelerate bone regeneration [65]. Selective killing of pre-OCs may lead to side effects such as nonunion of fracture. When using TXNRD1 inhibitors to treat osteoclast-related diseases or cancers, special attention should be given to PDGF-BB levels, and the dosing regimen should be adjusted accordingly. To demonstrate that it is TXNRD1 and not other targets of AF and TRi-1 that lead to the observations, TXNRD1 KO BMDMs are required for the following research. In addition, it has been reported that bone marrow stromal cells (BMSCs) effectively take up cystine and reduce it to cysteine, which is then released into the microenvironment for uptake by tumor cells to promote GSH synthesis [66]. In our experiments, the effects of the *in vivo* microenvironment on BMDMs and pre-OCs were not explored. Since cells import cysteine via the non-SLC7A11 pathway, high concentrations of cysteine in the microenvironment may directly affect the susceptibility of cells to TXNRD1 inhibitors or modulate SLC7A11 and other gene expressions to exert indirect effects. *In vitro* coculture of BMDMs and BMSCs may clarify the source of intracellular cysteine during osteoclast differentiation.

Together, our study found that TXNRD1 inhibitors cause cystine accumulation in mouse bone tissue, reduce the number of osteoclasts and alleviate bone loss in OVX mice. *In vitro* experiments showed that TXNRD1 inhibitors selectively killed pre-OCs. Cell death in this context was distinct from ferroptosis, ROS per se induced cell death, apoptosis, necroptosis, and autophagy. It is a novel form of cell death known as disulfidptosis, characterised by cystine accumulation and F-actin contraction. NFATc1-mediated upregulation of SLC7A11 leads to increased cystine uptake in pre-OCs and renders pre-OCs more sensitive to TXNRD1 inhibitors. Our study provides a new theoretical basis for AF, a canonical clinical drug, and suggests TXNRD1 inhibitors as a treatment for osteoclast-overactive diseases.

Author contributions

Zeyuan Zhong, Chongjing Zhang, and Baoqing Yu designed the study. Zeyuan Zhong, Shuo Ni and Zhi Qian performed the experiments and drafted the manuscript. Miao Ma, Weicong Sang, and Tao Lv analysed the data. Zhi Qian and Chengqing Yi gave the technical and material support. Xiaomeng Zhang, Chongjing Zhang and Baoqing Yu revised the paper. All authors read and approved the final manuscript.

Data availability statement

The datasets used and/or analysis during the current study are available from the corresponding author on reasonable request.

Declaration of competing interest

All authors declare no conflict of interests.

Acknowledgements

This work was supported by the Natural Science Foundation of China (82170897), Science and Technology Development Fund of Pudong New Area (PKJ2022-Y36), Gansu Provincial University Youth Doctoral Fund Project (2022QB-160), and Gansu Provincial University Innovation Fund Project (2022A-121).

Appendix A. Supplementary data

Supplementary data to this article can be found online at https://doi.org/10.1016/j.redox.2023.102711.

References

[1] T.D. Rachner, S. Khosla, L.C. Hofbauer, Osteoporosis: now and the future, Lancet 377 (9773) (2011) 1276–1287, https://doi.org/10.1016/S0140-6736(10)62349-5.
[2] S. Song, Y. Guo, Y. Yang, D. Fu, Advances in pathogenesis and therapeutic strategies for osteoporosis, Pharmacol. Ther. 237 (Sep. 2022), https://doi.org/10.1016/J.PHARMTHERA.2022.108168.
[3] Z. Chen, A. Bozec, A. Ramming, G. Schett, Anti-inflammatory and immune-regulatory cytokines in rheumatoid arthritis, Nat. Rev. Rheumatol. 15 (1) (Jan. 2019) 9–17, https://doi.org/10.1038/S41584-018-0109-2.
[4] N. Komatsu, H. Takayanagi, Mechanisms of joint destruction in rheumatoid arthritis - immune cell-fibroblast-bone interactions, Nat. Rev. Rheumatol. 18 (7) (Jul. 2022) 415–429, https://doi.org/10.1038/S41584-022-00793-5.
[5] R.E. Coleman, et al., Bone metastases, Nat. Rev. Dis. Prim. 6 (1) (Dec. 2020), https://doi.org/10.1038/S41572-020-00216-3.
[6] J.J. Yin, C.B. Pollock, K. Kelly, Mechanisms of cancer metastasis to the bone, Cell Res. 15 (1) (2005) 57–62, https://doi.org/10.1038/SJ.CR.7290266.
[7] W. Jiang, et al., PGE2 activates EP4 in subchondral bone osteoclasts to regulate osteoarthritis, Bone Res 10 (1) (Dec. 2022), https://doi.org/10.1038/s41413-022-00201-4.
[8] Y. Pang, et al., Metal-organic framework nanoparticles for ameliorating breast cancer-associated osteolysis, Nano Lett. 20 (2) (Feb. 2020) 829–840, https://doi.org/10.1021/acs.nanolett.9b02916.
[9] J. Luo, P. Sun, S. Siwko, M. Liu, J. Xiao, The role of GPCRs in bone diseases and dysfunctions, in: Bone Research, vol. 7, Sichuan University, Dec. 01, 2019, https://doi.org/10.1038/s41413-019-0059-6, 1.
[10] I.R. Reid, E.O. Billington, Drug therapy for osteoporosis in older adults, Lancet 399 (10329) (Mar. 2022) 1080–1092, https://doi.org/10.1016/S0140-6736(21)02646-5.
[11] Sci-Hub | DNA methyltransferase 3a regulates osteoclast differentiation by coupling to an S-adenosylmethionine–producing metabolic pathway. Nat. Med., 21 (3), 281–287 | 10.1038/nm.3774' (accessed October. 12, 2022)..
[12] S. Lucas, et al., Short-chain fatty acids regulate systemic bone mass and protect from pathological bone loss, Nat. Commun. 9 (1) (Dec. 2018), https://doi.org/10.1038/S41467-017-02490-4.
[13] K.H. Park-Min, Metabolic reprogramming in osteoclasts, Semin. Immunopathol. 41 (5) (Sep. 2019) 565–572, https://doi.org/10.1007/S00281-019-00757-0.
[14] M. Rashkovan, A. Ferrando, Metabolic dependencies and vulnerabilities in leukemia, Genes Dev. 33 (21–22) (Nov. 2019) 1460–1474, https://doi.org/10.1101/GAD.326470.119.
[15] T.T.T. Nguyen, et al., Aurora kinase A inhibition reverses the Warburg effect and elicits unique metabolic vulnerabilities in glioblastoma, Nat. Commun. 12 (1) (Dec. 2021), https://doi.org/10.1038/S41467-021-25501-X.

[16] X. Jiang, B.R. Stockwell, M. Conrad, Ferroptosis: mechanisms, biology and role in disease, Nat. Rev. Mol. Cell Biol. 22 (4) (Apr. 2021) 266–282, https://doi.org/10.1038/S41580-020-00324-8.
[17] J.A. Combs, G.M. Denicola, The non-essential amino acid cysteine becomes essential for tumor proliferation and survival, Cancers 11 (5) (May 2019), https://doi.org/10.3390/CANCERS11050678.
[18] X. Liu, et al., Cystine transporter regulation of pentose phosphate pathway dependency and disulfide stress exposes a targetable metabolic vulnerability in cancer, Nat. Cell Biol. 22 (4) (Apr. 2020) 476–486, https://doi.org/10.1038/s41556-020-0496-x.
[19] P. Koppula, Y. Zhang, L. Zhuang, B. Gan, Amino acid transporter SLC7A11/xCT at the crossroads of regulating redox homeostasis and nutrient dependency of cancer, in: Cancer Communications, vol. 38, John Wiley and Sons Inc, Dec. 01, 2018, https://doi.org/10.1186/S40880-018-0288-X, 1.
[20] B. Espinosa, E.S.J. Arnér, Thioredoxin-related protein of 14 kDa as a modulator of redox signalling pathways, Br. J. Pharmacol. 176 (4) (Feb. 2019) 544–553, https://doi.org/10.1111/BPH.14479.
[21] J. Lu, A. Holmgren, The thioredoxin antioxidant system, Free Radic. Biol. Med. 66 (Jan. 2014) 75–87, https://doi.org/10.1016/J.FREERADBIOMED.2013.07.036.
[22] G. Bjørklund, L. Zou, J. Wang, C.T. Chasapis, M. Peana, Thioredoxin reductase as a pharmacological target, in: Pharmacological Research, vol. 174, Academic Press, Dec. 01, 2021, https://doi.org/10.1016/j.phrs.2021.105854.
[23] S. Urig, K. Becker, On the potential of thioredoxin reductase inhibitors for cancer therapy, Semin. Cancer Biol. 16 (6) (Dec. 2006) 452–465, https://doi.org/10.1016/j.semcancer.2006.09.004.
[24] W.C. Stafford, et al., Irreversible inhibition of cytosolic thioredoxin reductase 1 as a mechanistic basis for anticancer therapy [Online]. Available: http://stm.sciencemag.org/, 2018.
[25] X. Liu, et al., Actin cytoskeleton vulnerability to disulfide stress mediates disulfidptosis, Nat. Cell Biol. 25 (3) (Mar. 2023), https://doi.org/10.1038/S41556-023-01091-2.
[26] X. Yan, et al., Inhibition of thioredoxin/thioredoxin reductase induces synthetic lethality in lung cancers with compromised glutathione homeostasis, Cancer Res. 79 (1) (Jan. 2019) 125–132, https://doi.org/10.1158/0008-5472.CAN-18-1938.
[27] P. Sabatier, C.M. Beusch, R. Gencheva, Q. Cheng, R. Zubarev, E.S.J. Arnér, Comprehensive chemical proteomics analyses reveal that the new TRi-1 and TRi-2 compounds are more specific thioredoxin reductase 1 inhibitors than auranofin, Redox Biol. 48 (Dec. 2021), https://doi.org/10.1016/j.redox.2021.102184.
[28] J.L. Abruzzo, Auranofin: a new drug for rheumatoid arthritis, Ann. Intern. Med. 105 (2) (1986) 274–276, https://doi.org/10.7326/0003-4819-105-2-274.
[29] L. Yang, et al., Auranofin mitigates systemic iron overload and induces ferroptosis via distinct mechanisms, Signal Transduct. Targeted Ther. 5 (1) (Dec. 2020), https://doi.org/10.1038/s41392-020-00253-0.
[30] T. Gamberi, G. Chiappetta, T. Fiaschi, A. Modesti, F. Sorbi, F. Magherini, Upgrade of an old drug: auranofin in innovative cancer therapies to overcome drug resistance and to increase drug effectiveness, Med. Res. Rev. 42 (3) (May 2022) 1111–1146, https://doi.org/10.1002/MED.21872.
[31] L. Freire Boullosa, et al., Auranofin reveals therapeutic anticancer potential by triggering distinct molecular cell death mechanisms and innate immunity in mutant p53 non-small cell lung cancer, Redox Biol. 42 (Jun. 2021), https://doi.org/10.1016/J.REDOX.2021.101949.
[32] N.H. Kim, M.Y. Lee, S.J. Park, J.S. Choi, M.K. Oh, I.S. Kim, Auranofin blocks interleukin-6 signalling by inhibiting phosphorylation of JAK1 and STAT3, Immunology 122 (4) (Dec. 2007) 607–614, https://doi.org/10.1111/J.1365-2567.2007.02679.X.
[33] H.S. Youn, J.Y. Lee, S.I. Saitoh, K. Miyake, D.H. Hwang, Auranofin, as an anti-rheumatic gold compound, suppresses LPS-induced homodimerization of TLR4, Biochem. Biophys. Res. Commun. 350 (4) (Dec. 2006) 866–871, https://doi.org/10.1016/J.BBRC.2006.09.097.
[34] H. Hwangbo, et al., Anti-inflammatory effect of auranofin on palmitic acid and LPS-induced inflammatory response by modulating TLR4 and NOX4-mediated NF-κB signaling pathway in RAW264.7 macrophages, Int. J. Mol. Sci. 22 (11) (Jun. 2021), https://doi.org/10.3390/IJMS22115920.
[35] H.Y. Kim, K.S. Kim, M.J. Kim, H.S. Kim, K.Y. Lee, K.W. Kang, Auranofin inhibits RANKL-induced osteoclastogenesis by suppressing inhibitors of κ B kinase and inflammasome-mediated interleukin-1 β secretion, Oxid. Med. Cell. Longev. 2019 (2019), https://doi.org/10.1155/2019/3503912.
[36] S. Tian, F.M. Siu, C.N. Lok, Y.M.E. Fung, C.M. Che, Anticancer auranofin engages 3-hydroxy-3-methylglutaryl-coenzyme A reductase (HMGCR) as a target, Metallomics 11 (11) (Nov. 2019) 1925–1936, https://doi.org/10.1039/C9MT00185A.
[37] A. de Luca, C.G. Hartinger, P.J. Dyson, M. lo Bello, A. Casini, A new target for gold (I) compounds: glutathione-S-transferase inhibition by auranofin, J. Inorg. Biochem. 119 (Feb. 2013) 38–42, https://doi.org/10.1016/J.JINORGBIO.2012.08.006.
[38] F. Fata, et al., Biochemical and structural characterizations of thioredoxin reductase selenoproteins of the parasitic filarial nematodes Brugia malayi and Onchocerca volvulus, Redox Biol. 51 (May 2022), https://doi.org/10.1016/J.REDOX.2022.102278.
[39] C. Zhang, et al., The dibenzyl isoquinoline alkaloid berbamine ameliorates osteoporosis by inhibiting bone resorption, Front. Endocrinol. 13 (May 2022), https://doi.org/10.3389/FENDO.2022.885507.
[40] L. Zhang, et al., Highly selective off-on fluorescent probe for imaging thioredoxin reductase in living cells, J. Am. Chem. Soc. 136 (1) (Jan. 2014) 226–233, https://doi.org/10.1021/JA408792K.
[41] A. Jamalpoor, et al., Cysteamine–bicalutamide combination therapy corrects proximal tubule phenotype in cystinosis, EMBO Mol. Med. 13 (7) (Jul. 2021), https://doi.org/10.15252/emmm.202013067.
[42] H.S. Kaya-Okur, et al., CUT&Tag for efficient epigenomic profiling of small samples and single cells, Nat. Commun. 10 (1) (Dec. 2019), https://doi.org/10.1038/S41467-019-09982-5.
[43] J.G. Felber, et al., Cyclic 5-membered disulfides are not selective substrates of thioredoxin reductase, but are opened nonspecifically, Nat. Commun. 13 (1) (Dec. 2022), https://doi.org/10.1038/S41467-022-29136-4.
[44] I. Padera, et al., Thioredoxin-related protein of 14 kDa is an efficient L-cystine reductase and S-denitrosylase, Proc. Natl. Acad. Sci. U. S. A. 111 (19) (May 2014) 6964–6969, https://doi.org/10.1073/PNAS.1317320111.
[45] H. Kanzaki, F. Shinohara, M. Kajiya, T. Kodama, The Keap1/Nrf2 protein axis plays a role in osteoclast differentiation by regulating intracellular reactive oxygen species signaling, J. Biol. Chem. 288 (32) (Aug. 2013) 23009–23020, https://doi.org/10.1074/jbc.M113.478545.
[46] E. Habib, K. Linher-Melville, H.X. Lin, G. Singh, Expression of xCT and activity of system xc(-) are regulated by NRF2 in human breast cancer cells in response to oxidative stress, Redox Biol. 5 (Aug. 2015) 33–42, https://doi.org/10.1016/J.REDOX.2015.03.003.
[47] G. Lei, et al., The role of ferroptosis in ionizing radiation-induced cell death and tumor suppression, Cell Res. 30 (2) (Feb. 2020) 146–162, https://doi.org/10.1038/S41422-019-0263-3.
[48] Z. Fan, et al., Nrf2-Keap1 pathway promotes cell proliferation and diminishes ferroptosis, Oncogenesis 6 (8) (2017), https://doi.org/10.1038/ONCSIS.2017.65.
[49] L. Penolazzi, et al., Induction of estrogen receptor α expression with decoy oligonucleotide targeted to NFATc1 binding sites in osteoblasts, Mol. Pharmacol. 71 (6) (Jun. 2007) 1457–1462, https://doi.org/10.1124/mol.107.034561.
[50] M. Ashtar, et al., The roles of ROS generation in RANKL-induced osteoclastogenesis: suppressive effects of febuxostat, Cancers 12 (4) (Apr. 2020), https://doi.org/10.3390/cancers12040929.
[51] K.V. Floros, et al., MYCN-amplified neuroblastoma is addicted to iron and vulnerable to inhibition of the system xc-/glutathione Axis, Cancer Res. 81 (7) (Apr. 2021) 1896–1908, https://doi.org/10.1158/0008-5472.CAN-20-1641.
[52] Z. Zhong, et al., Tetrandrine prevents bone loss in ovariectomized mice by inhibiting RANKL-induced osteoclastogenesis, Front. Pharmacol. 10 (2020), https://doi.org/10.3389/fphar.2019.01530.
[53] F. Zhang, et al., Juglanin inhabits osteoclastogenesis in ovariectomized mice via the suppression of NF-κB signaling pathways I n r e v i e w [Online]. Available: www.frontiersin.org.
[54] S. Ni, et al., Schisandrin A restrains osteoclastogenesis by inhibiting reactive oxygen species and activating Nrf2 signalling, Cell Prolif. 53 (10) (Oct. 2020), https://doi.org/10.1111/cpr.12882.
[55] H.Y. Kim, K.S. Kim, M.J. Kim, H.S. Kim, K.Y. Lee, K.W. Kang, Auranofin inhibits RANKL-induced osteoclastogenesis by suppressing inhibitors of κB kinase and inflammasome-mediated interleukin-1β secretion, Oxid. Med. Cell. Longev. 2019 (2019), https://doi.org/10.1155/2019/3503912.
[56] T.J. Hall, H. Jeker, H. Nyugen, M. Schaeublin, Gold Salts Inhibit Osteoclastic Bone Resorption in Vitro, 1996.
[57] W. Wang, et al., Inhibition of Syk promotes chemical reprogramming of fibroblasts via metabolic rewiring and H 2 S production, EMBO J. 40 (11) (Jun. 2021), https://doi.org/10.15252/embj.2020106771.
[58] M.K. Srivastava, P. Sinha, V.K. Clements, P. Rodriguez, S. Ostrand-Rosenberg, Myeloid-derived suppressor cells inhibit T-cell activation by depleting cystine and cysteine, Cancer Res. 70 (1) (Jan. 2010) 68–77, https://doi.org/10.1158/0008-5472.CAN-09-2587.
[59] P.J. Siska, et al., Fluorescence-based measurement of cystine uptake through xCT shows requirement for ROS detoxification in activated lymphocytes, J. Immunol. Methods 438 (Nov. 2016) 51–58, https://doi.org/10.1016/J.JIM.2016.08.013.
[60] C. Procaccini, et al., Signals of pseudo-starvation unveil the amino acid transporter SLC7A11 as key determinant in the control of Treg cell proliferative potential, Immunity 54 (7) (Jul. 2021) 1543–1560, https://doi.org/10.1016/J.IMMUNI.2021.04.014, e6.
[61] N. Liu, et al., Clinically used antirheumatic agent auranofin is a proteasomal deubiquitinase inhibitor and inhibits tumor growth, Oncotarget 5 (14) (2014) 5453–5471, https://doi.org/10.18632/ONCOTARGET.2113.
[62] B.F. Boyce, Advances in the regulation of osteoclasts and osteoclast functions, J. Dent. Res. 92 (10) (Oct. 2013) 860–867, https://doi.org/10.1177/0022034513500306.
[63] Z. Tang, et al., HO-1-mediated ferroptosis as a target for protection against retinal pigment epithelium degeneration, Redox Biol. 43 (Jul. 2021), https://doi.org/10.1016/j.redox.2021.101971.
[64] X. Lang, et al., Radiotherapy and immunotherapy promote tumoral lipid oxidation and ferroptosis via synergistic repression of SLC7A11, Cancer Discov. 9 (12) (Dec. 2019) 1673–1685, https://doi.org/10.1158/2159-8290.CD-19-0338.
[65] H. Xie, et al., PDGF-BB secreted by preosteoclasts induces angiogenesis during coupling with osteogenesis, Nat. Med. 20 (11) (2014) 1270–1278, https://doi.org/10.1038/nm.3668.
[66] W. Zhang, et al., Stromal control of cystine metabolism promotes cancer cell survival in chronic lymphocytic leukaemia, Nat. Cell Biol. 14 (3) (Mar. 2012) 276–286, https://doi.org/10.1038/ncb2432.